SUPPORTING INFORMATION

New azo-decorated *N*-pyrrolidinylthiazoles: synthesis, properties and an unexpected remote substituents effect transmission

Carla Boga,*[a] Silvia Cino,[a] Gabriele Micheletti,[a] Daniele Padovan,[a] Luca Prati,[a] Andrea Mazzanti,[a] Nicola Zanna[a]

Department of Industrial Chemistry 'Toso Montanari', ALMA MATER STUDIORUM - Università di Bologna, Viale del Risorgimento, 4 40136 Bologna, Italy

Corresponding author e-mail: carla.boga@unibo.it

Content **Page**

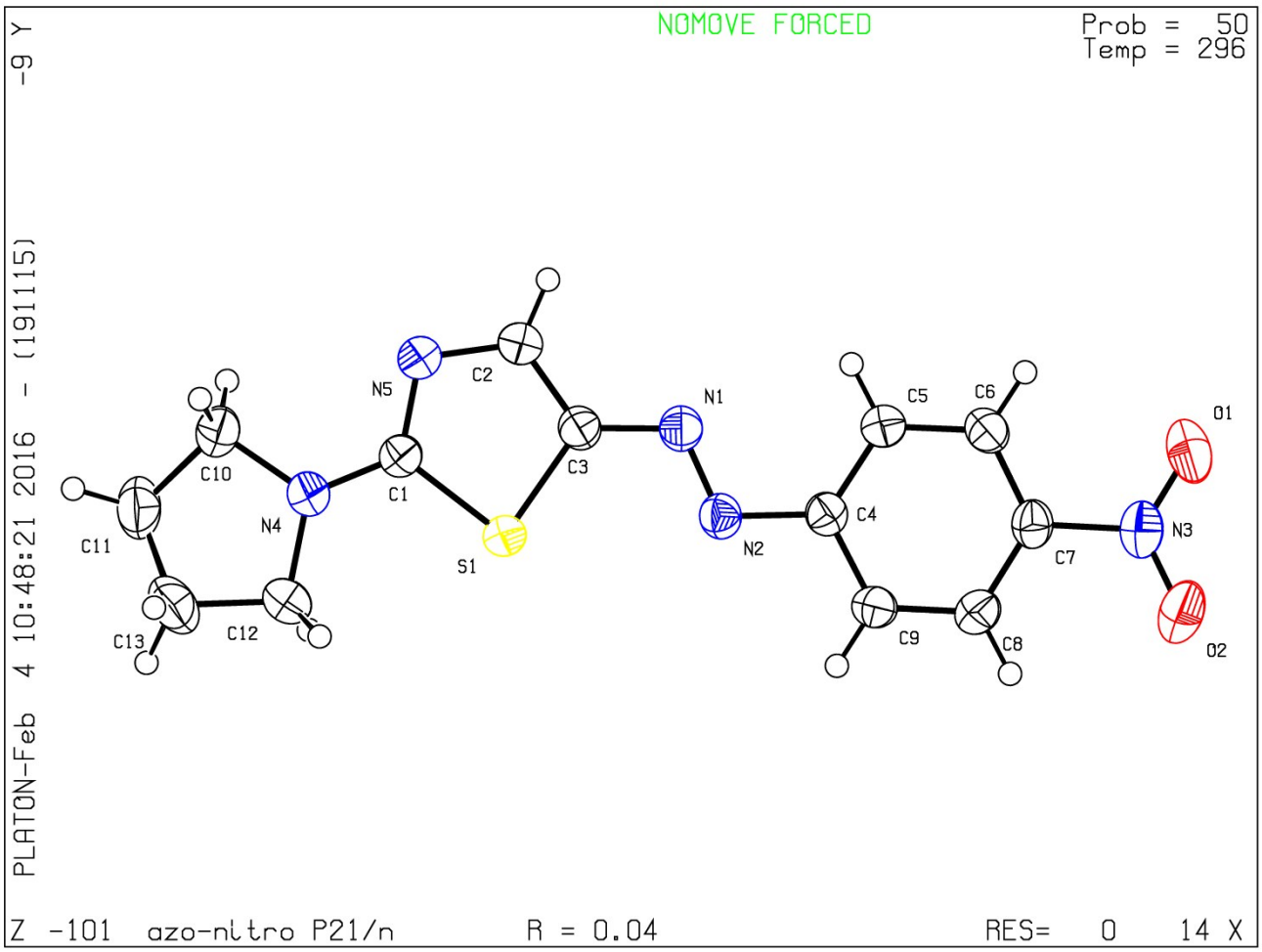

Fig. SI-1. ORTEP representation for 5a

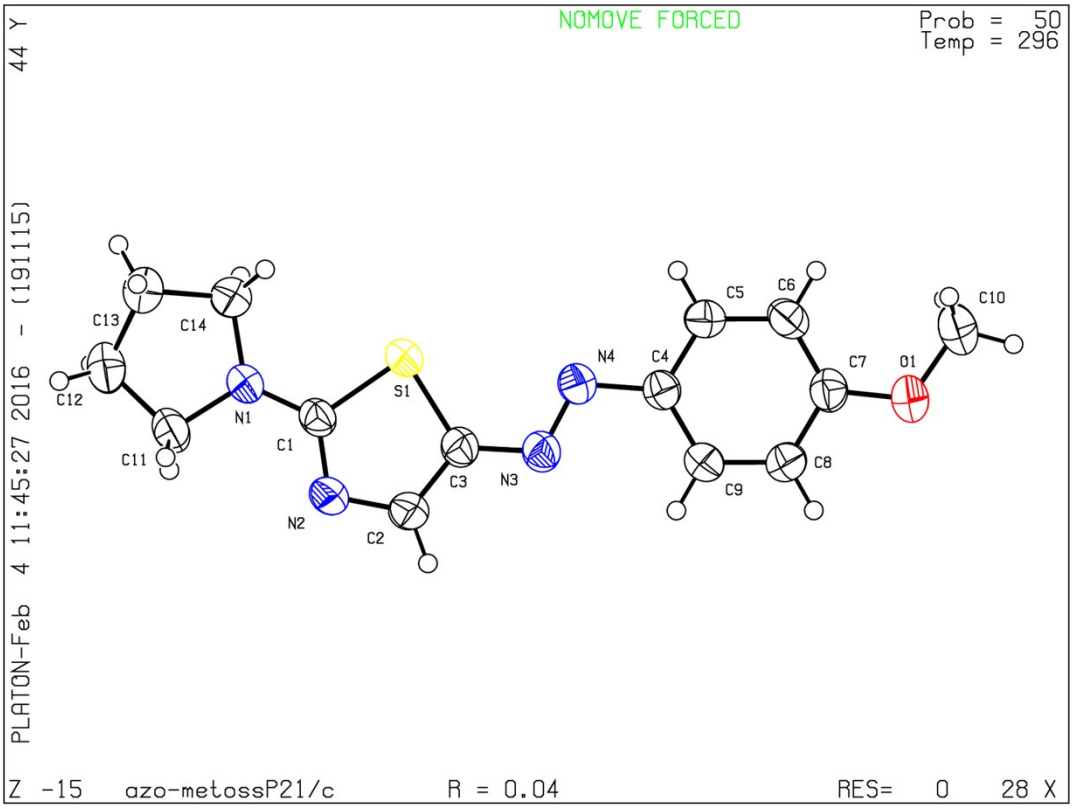

Fig. SI-2. ORTEP representation for 5c

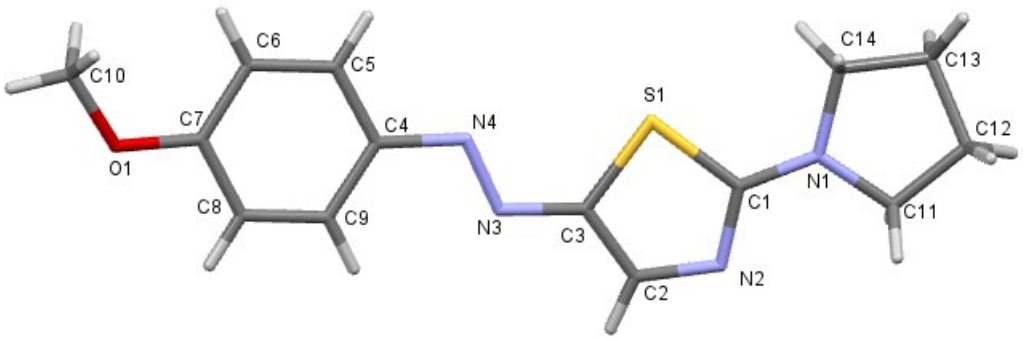

Figure SI-3. Graphic representation of the crystalline structure of compound **5c**.

VT-NMR DATA

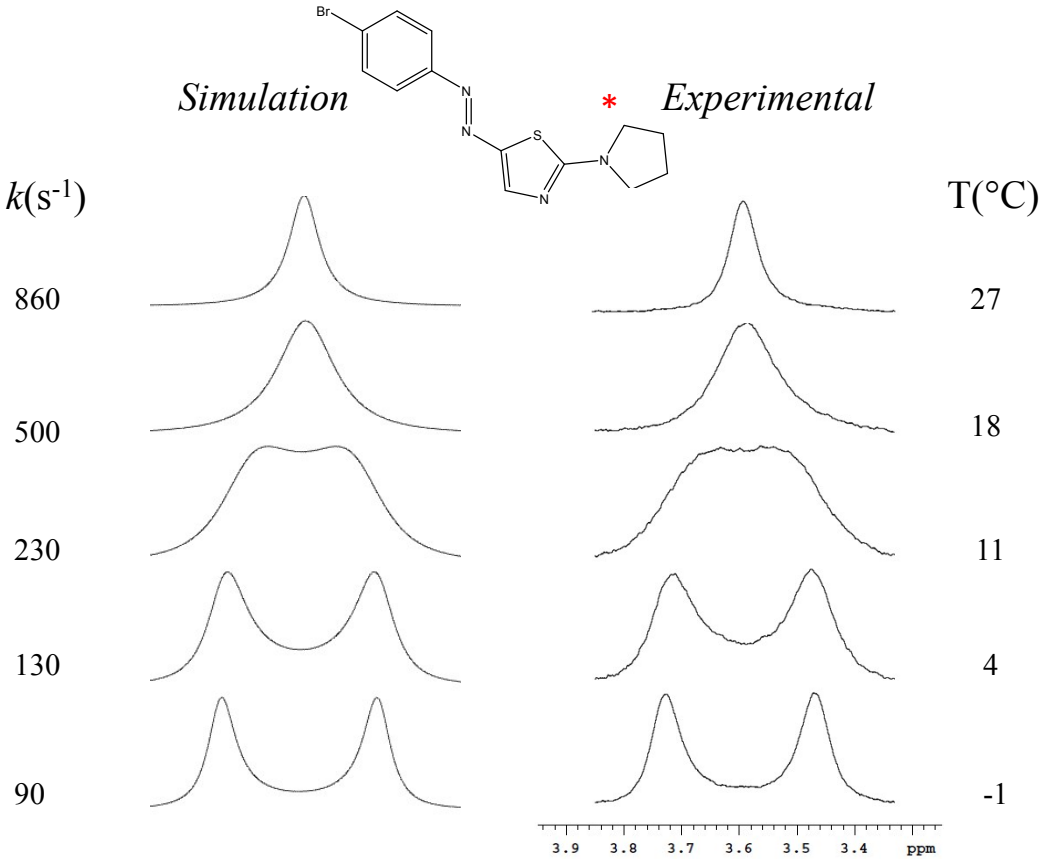

$\Delta G^{\ddagger} = 13{,}5 \pm 0{,}2$ kcal/mol

Figure SI-4. Methylene variable temperature ^{1}H-NMR spectra in $CDCl_3$ and dynamic-NMR simulations for **5b**.

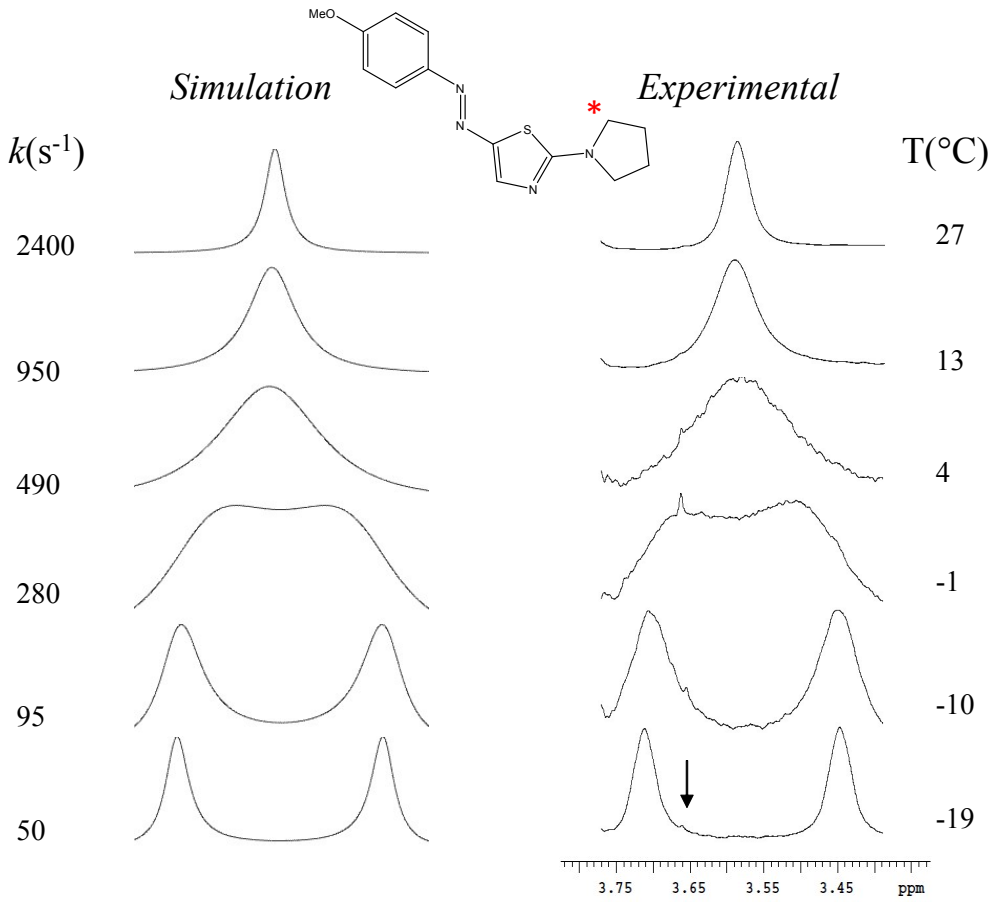

$\Delta G^{\ddagger} = 12{,}9 \pm 0{,}2$ kcal/mol

Figure SI-5. Methylene variable temperature ^{1}H-NMR spectra in $CDCl_3$ and dynamic-NMR simulations for **5c**. Black arrows indicates impurity.

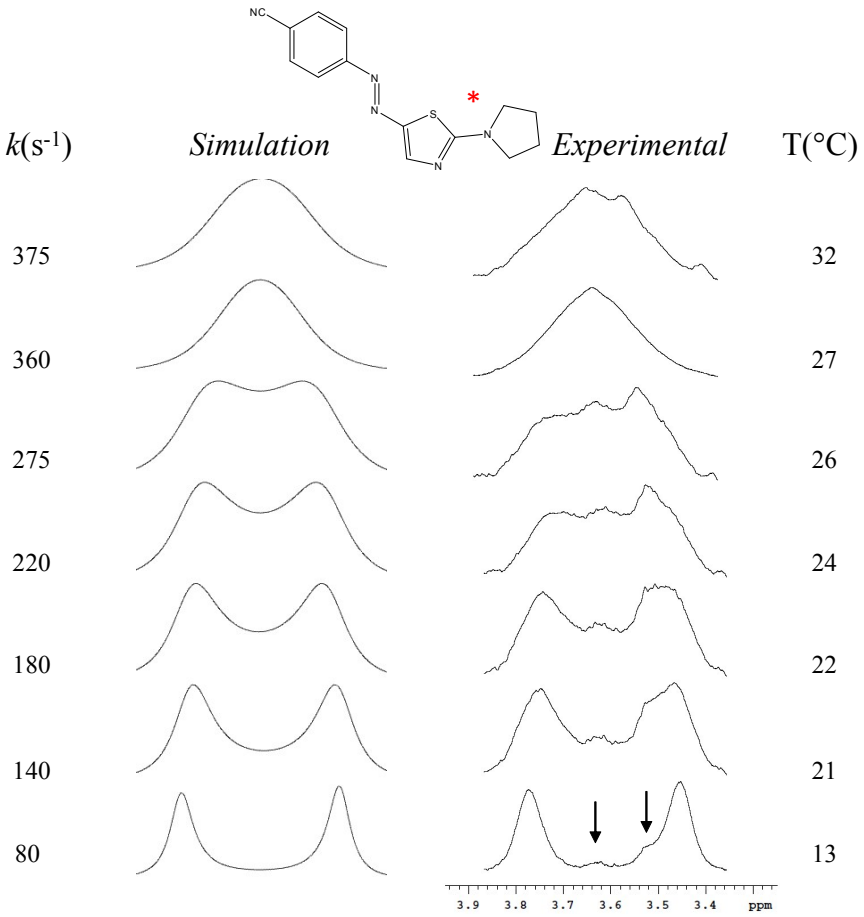

$\Delta G^{\ddagger} = 14{,}2 \pm 0{,}2$ kcal/mol

Figure SI-6. Methylene variable temperature ^{1}H-NMR spectra in $CDCl_3$ and dynamic-NMR simulations for **5d**. Black arrows indicates impurity.

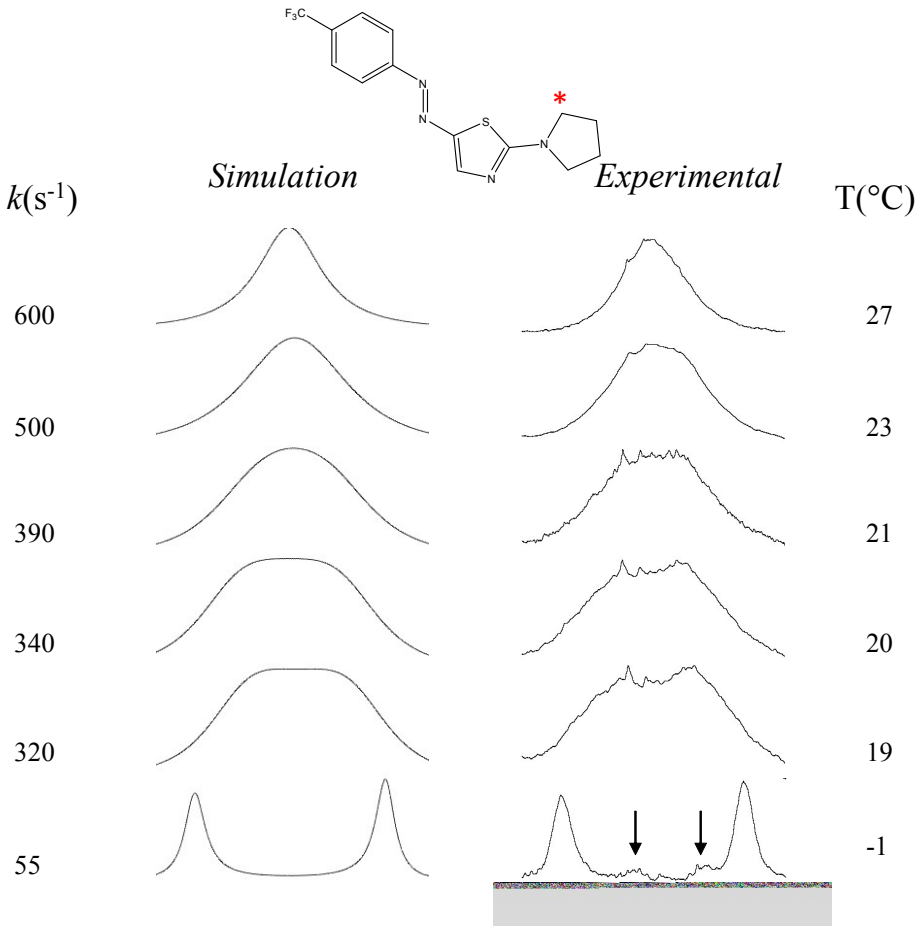

Figure SI-7. Methylene variable temperature ^{1}H-NMR spectra in $CDCl_3$ and dynamic-NMR simulations for **5e**. Black arrows indicates impurity.

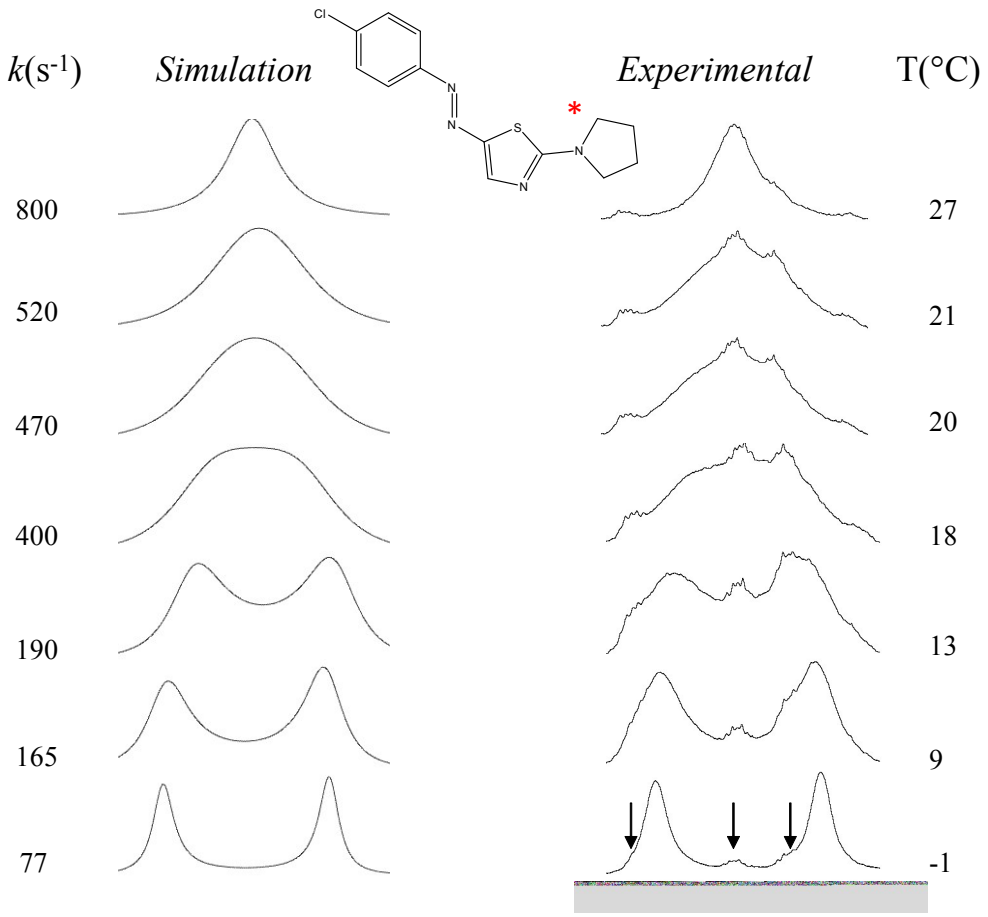

$\Delta G^{\ddagger} = 13{,}6 \pm 0{,}2$ kcal/mol

Figure SI-8. Methylene variable temperature ^{1}H-NMR spectra in $CDCl_3$ and dynamic-NMR simulations for **5f**. Black arrows indicates impurity.

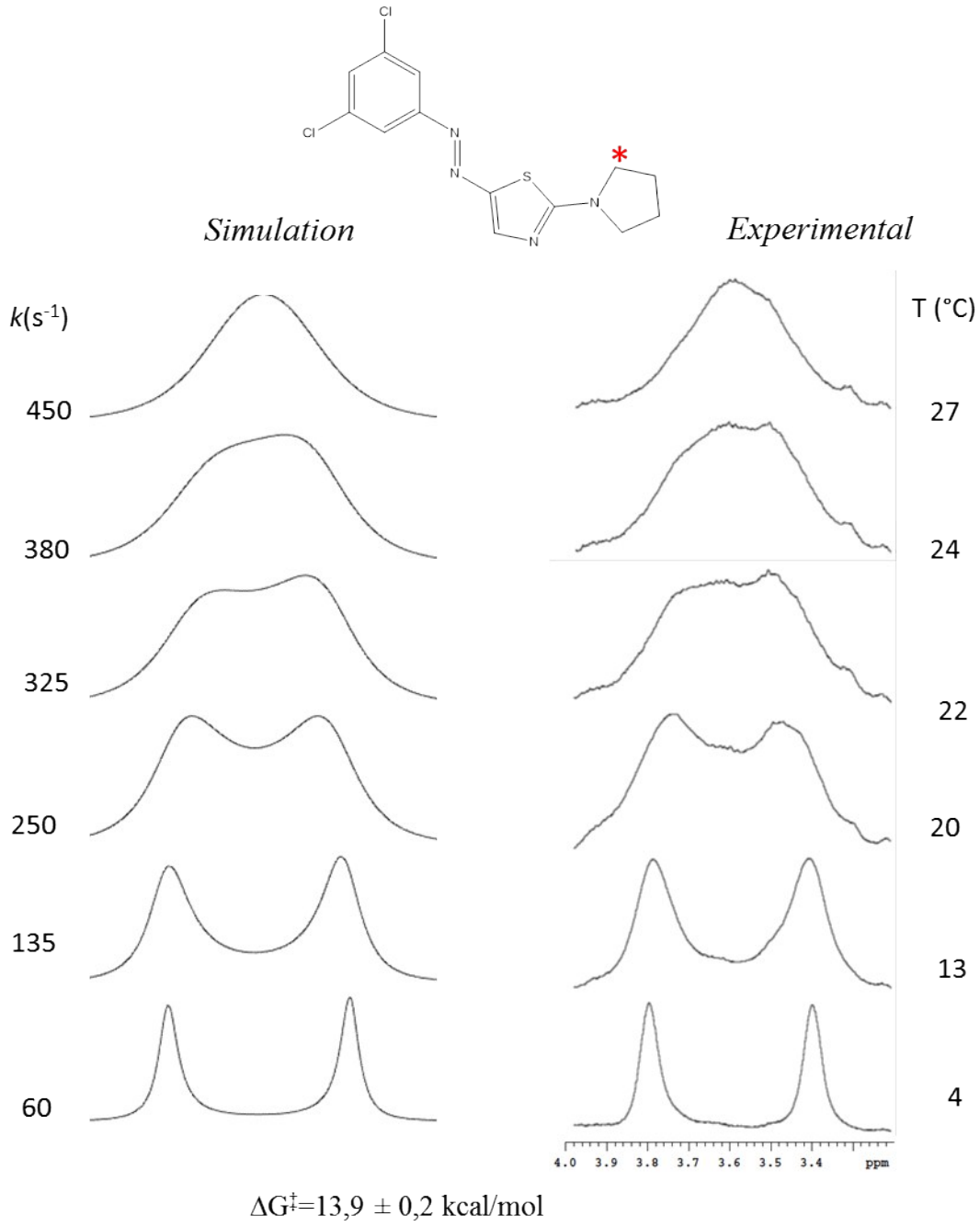

Figure SI-9. Methylene variable temperature ^{1}H-NMR spectra in $CDCl_3$ and dynamic-NMR simulations for **5g**.

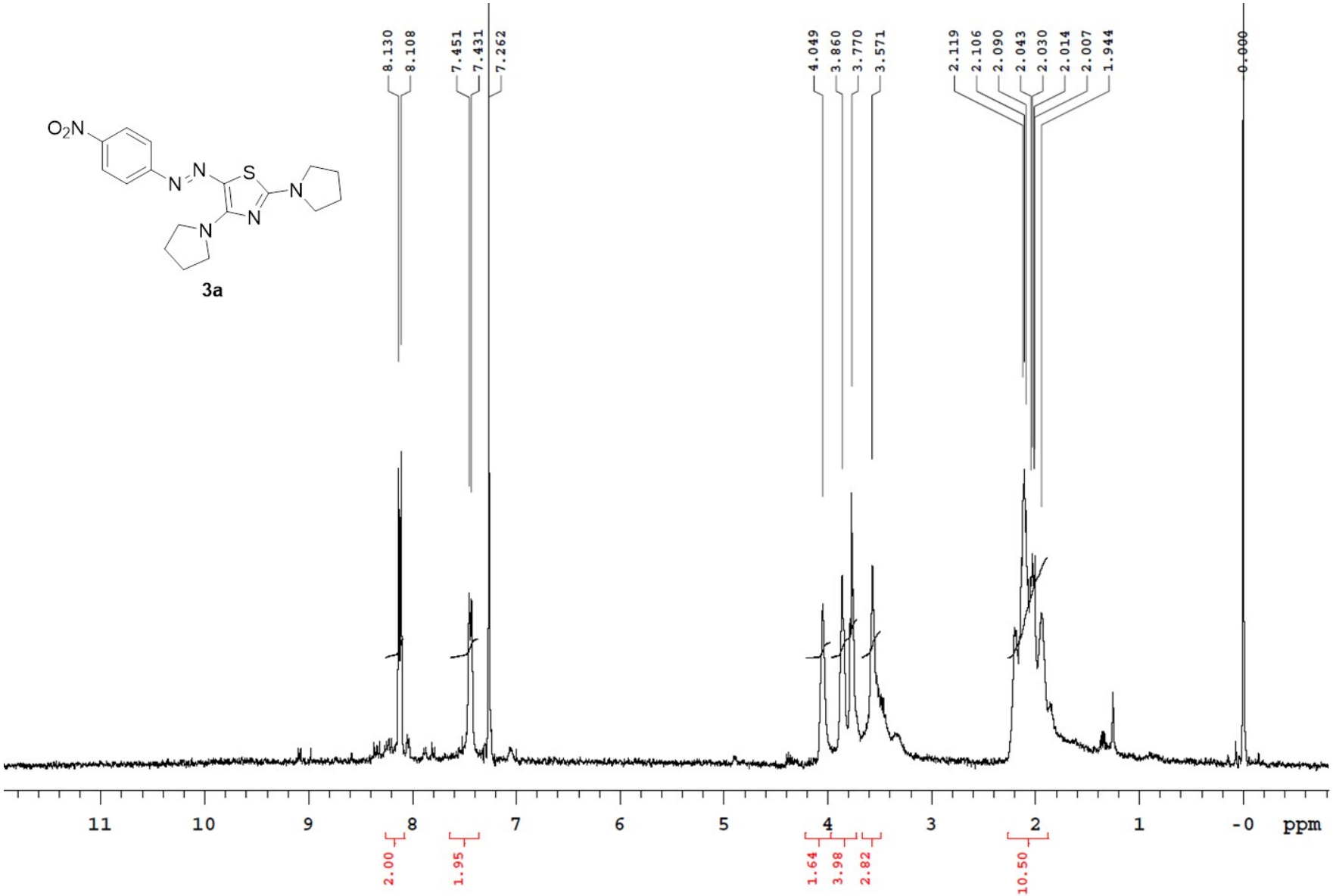

Fig. SI-10. ^{1}H NMR ($CDCl_3$, 400 MHz, 25 °C) spectrum of compound **3a**.

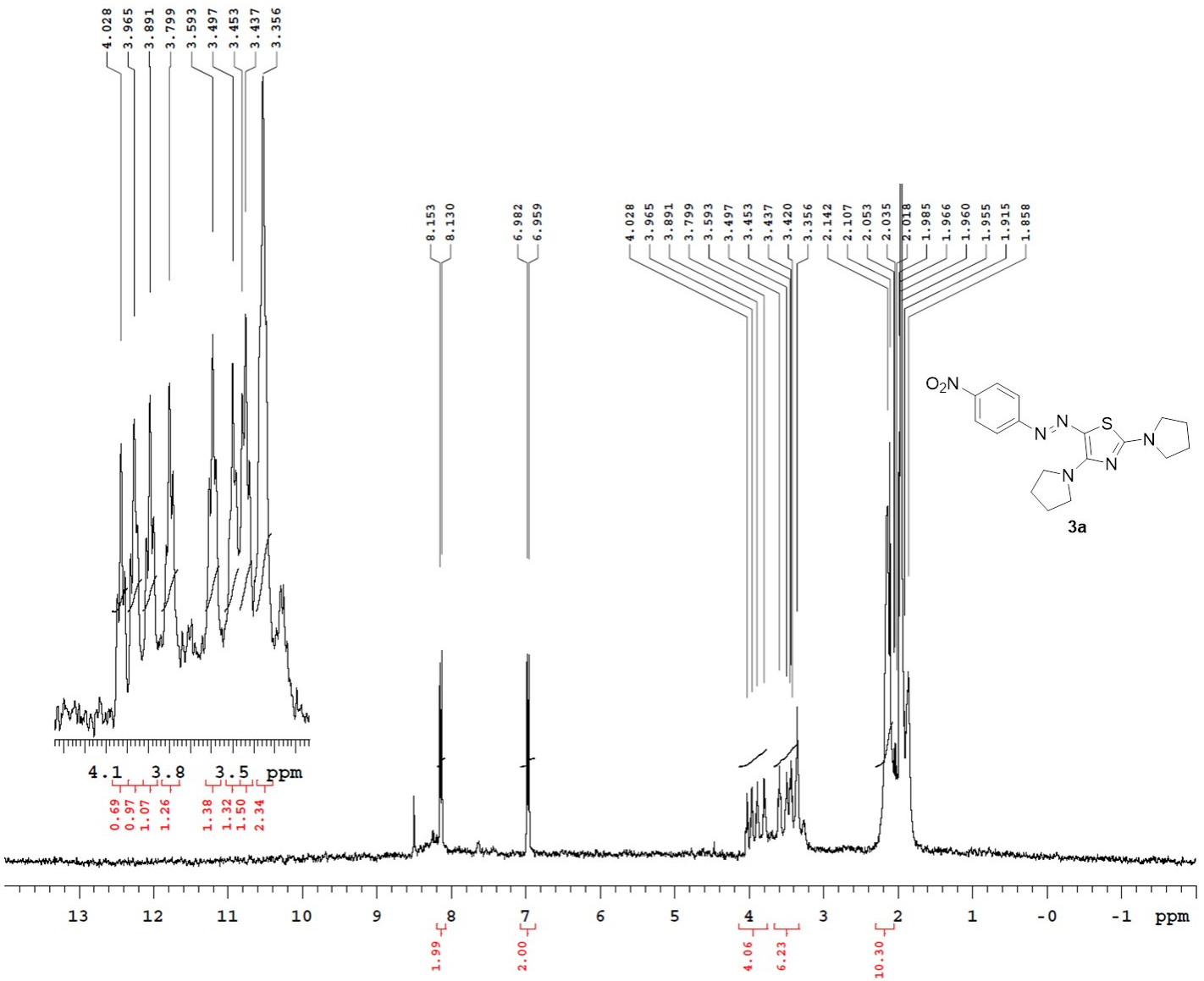

Fig. SI-11. ^{1}H NMR (CD_3CN, 400 MHz, 25 °C) spectrum of compound **3a**.

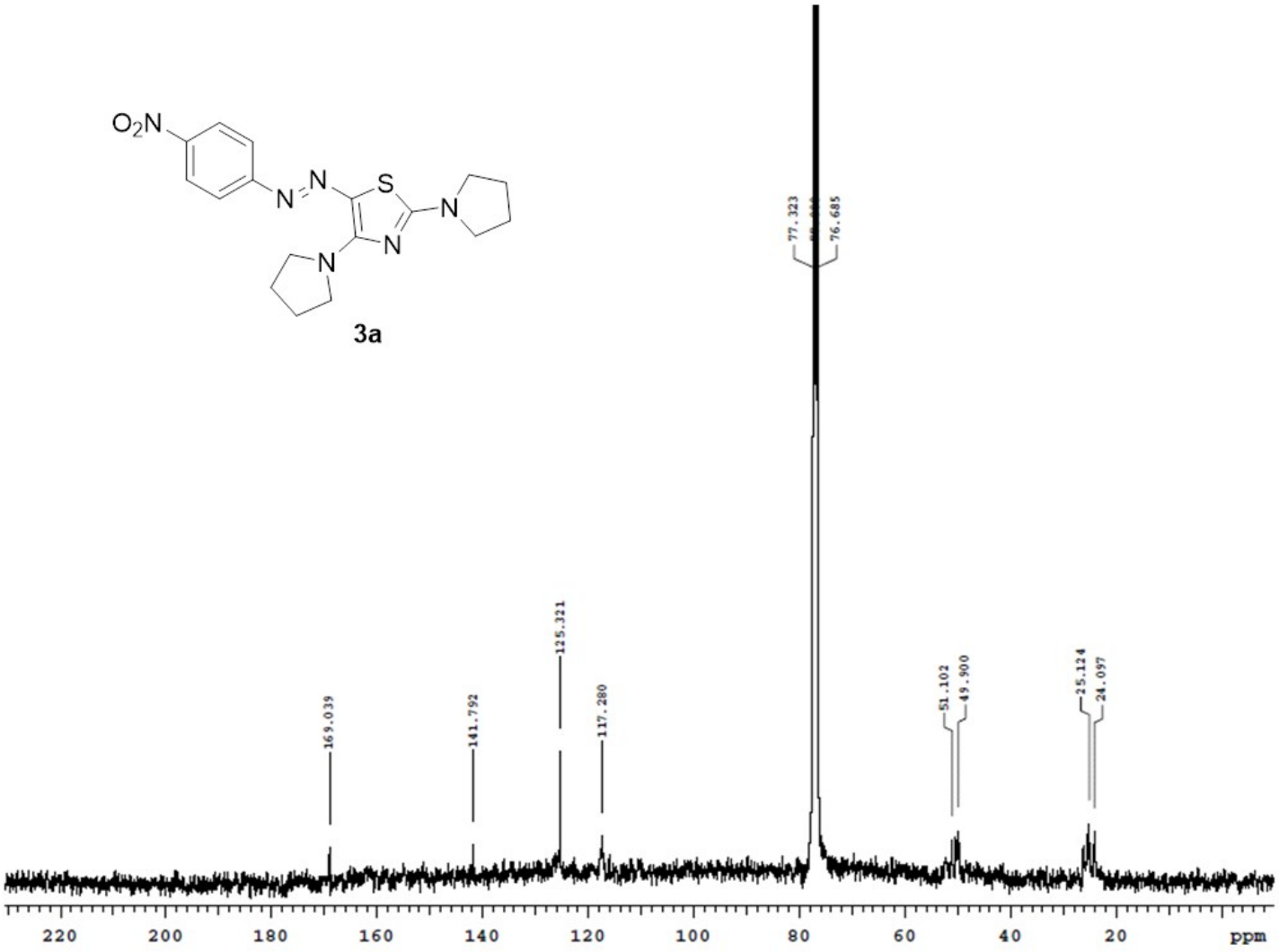

Fig. SI-12. ^{13}C NMR ($CDCl_3$, 100.56 MHz, 25 °C) spectrum of compound **3a.**

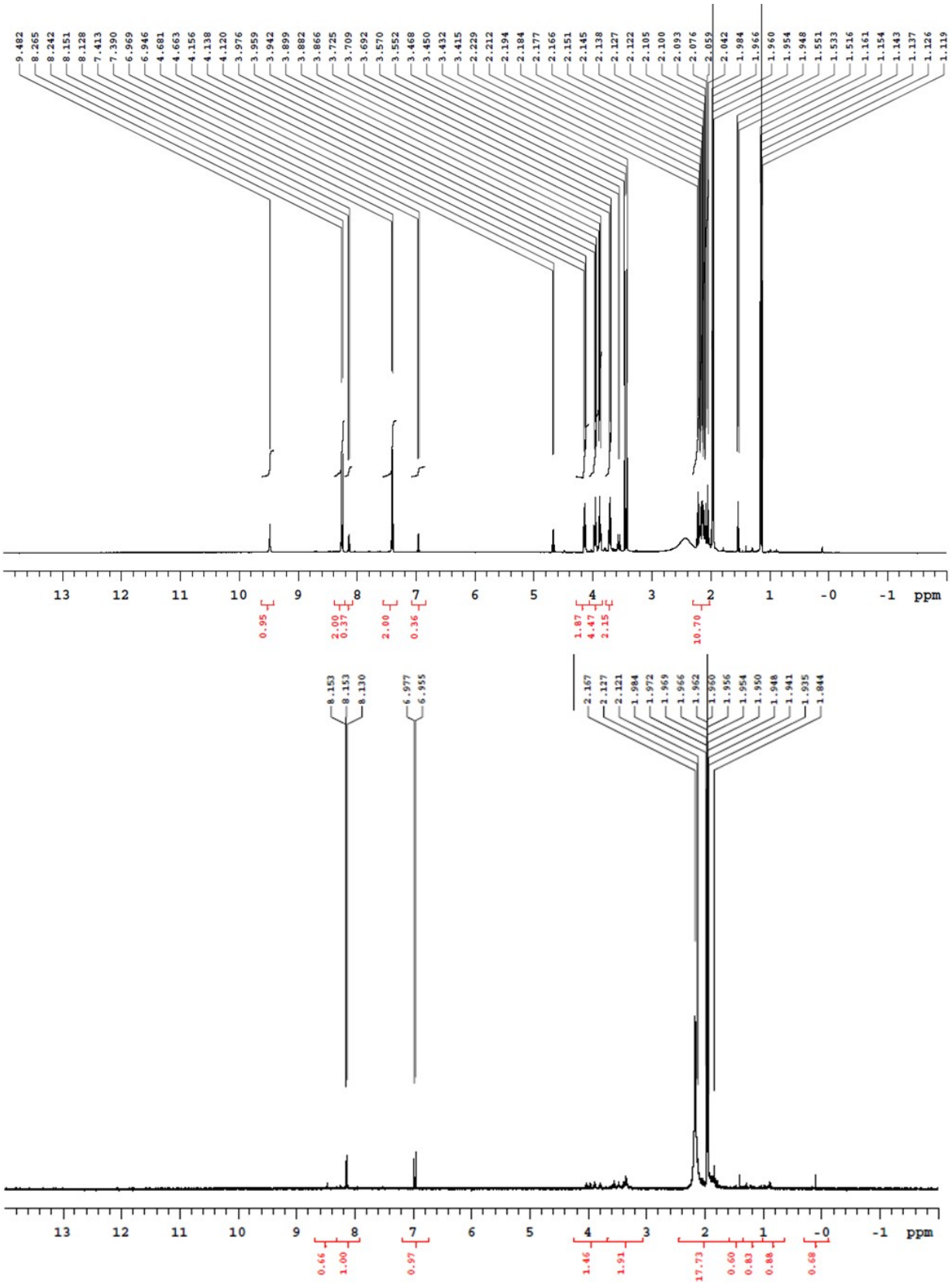

Fig. SI-13. ^{1}H NMR (CD_3CN, 400 MHz, 25 °C) spectrum of compound **3a** before (bottom) and after (top) addition of HBF_4/Et_2O with formation of **3aH**.

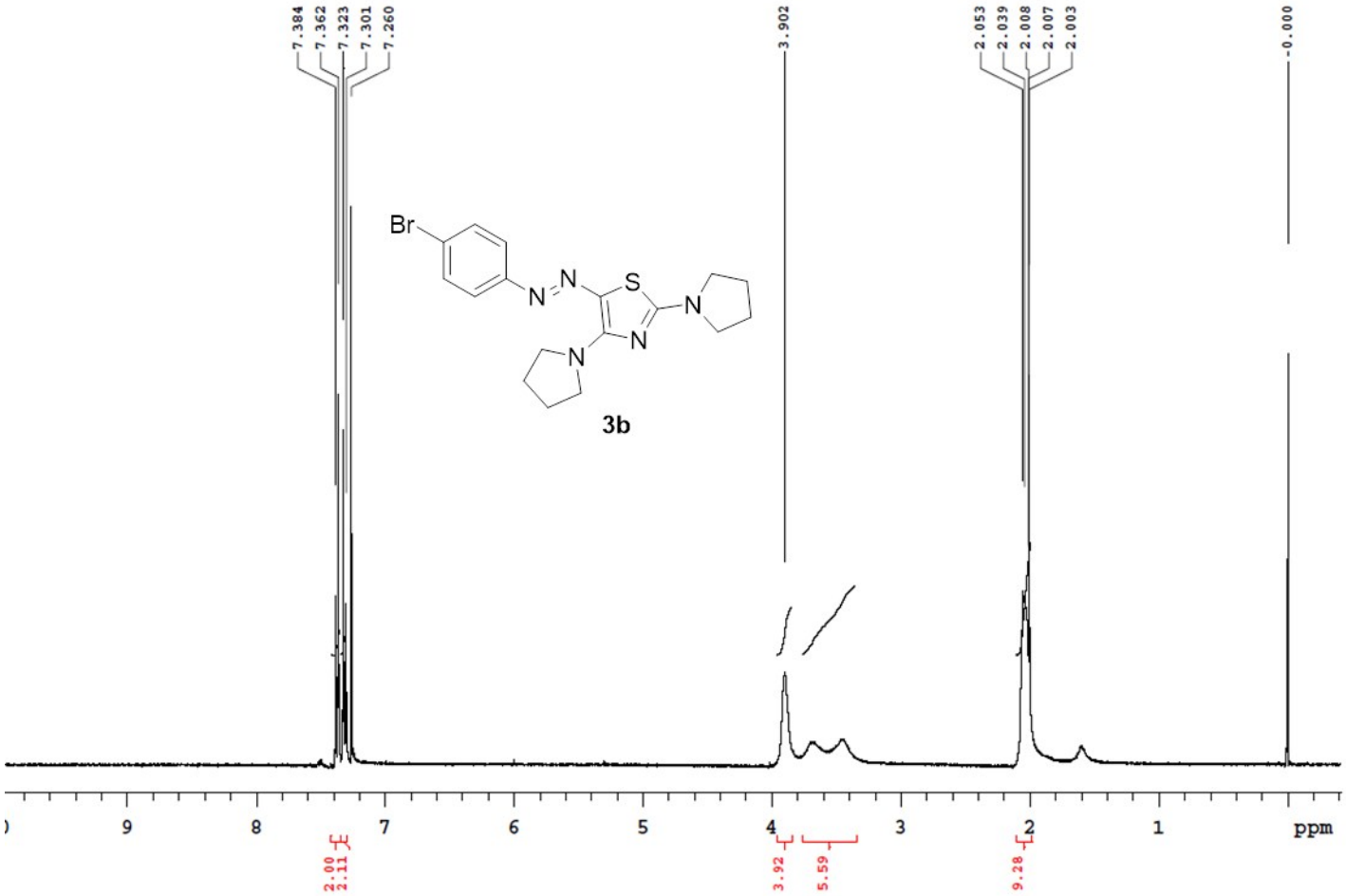

Fig. SI-14. ^{1}H NMR ($CDCl_3$, 400 MHz, 25 °C) spectrum of compound **3b.**

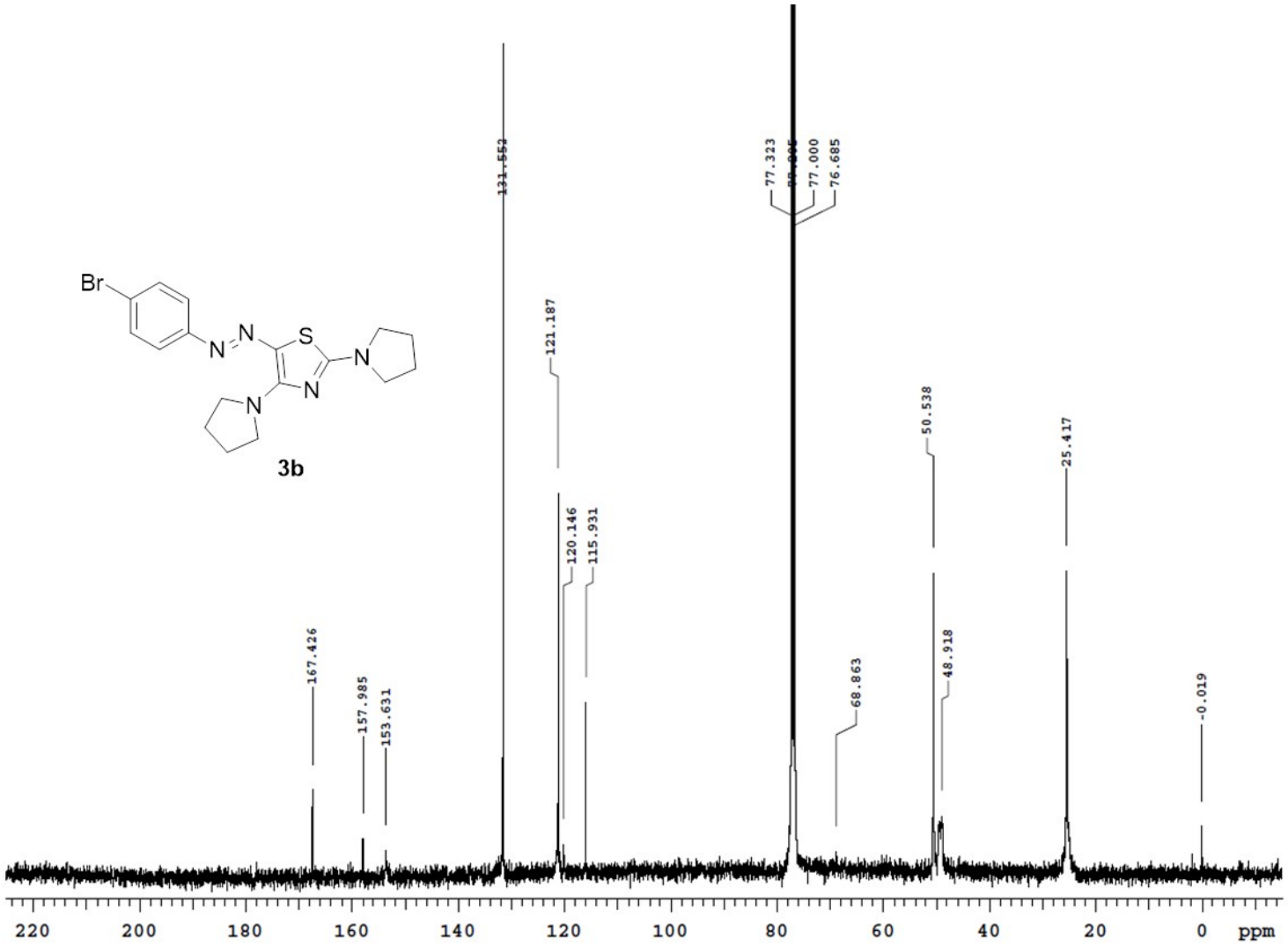

Fig. SI-15. ^{13}C NMR ($CDCl_3$, 100.56 MHz, 25 °C) spectrum of compound **3b.**

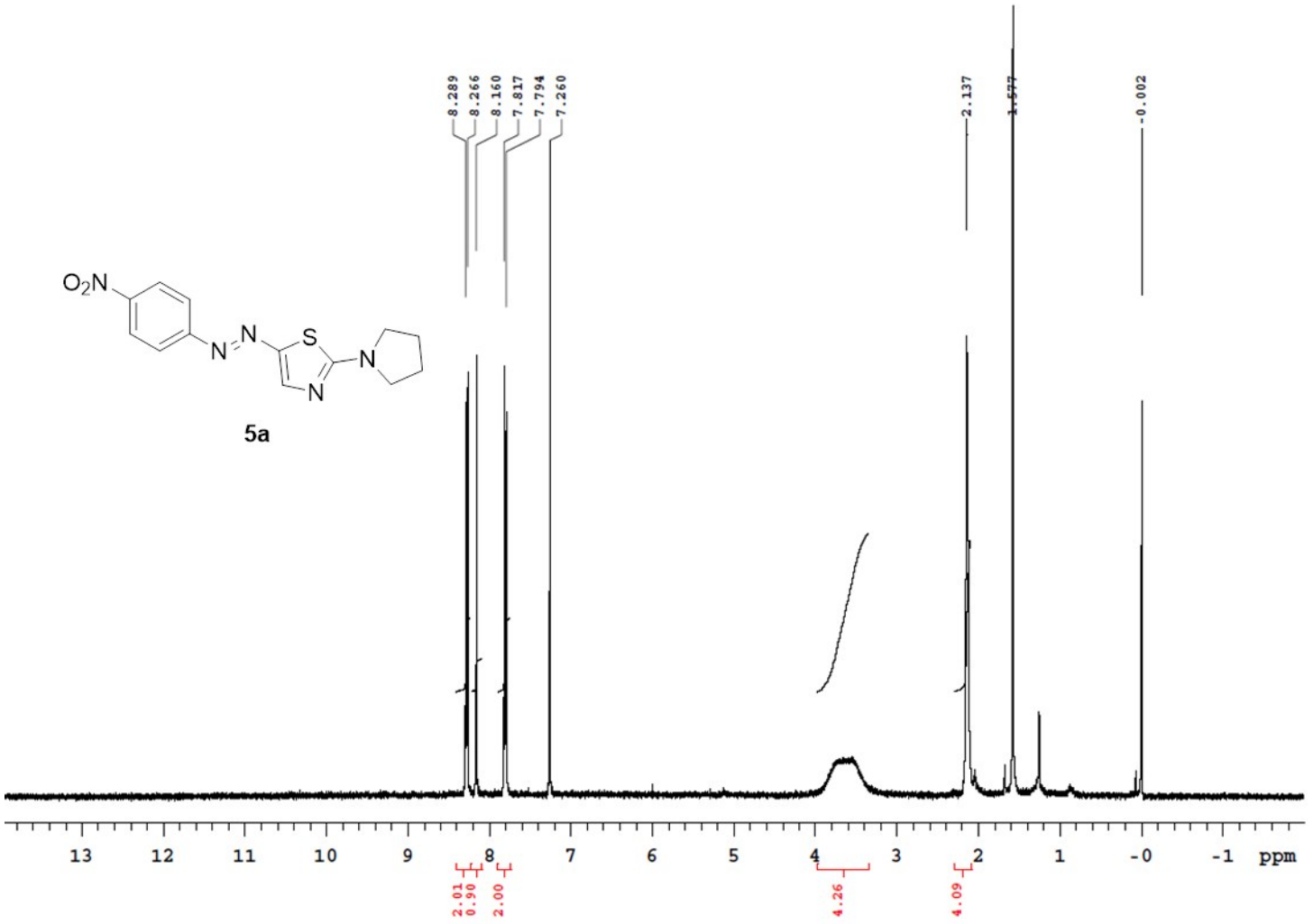

Fig. SI-16. ^{1}H NMR ($CDCl_3$, 400 MHz, 25 °C) spectrum of compound **5a.**

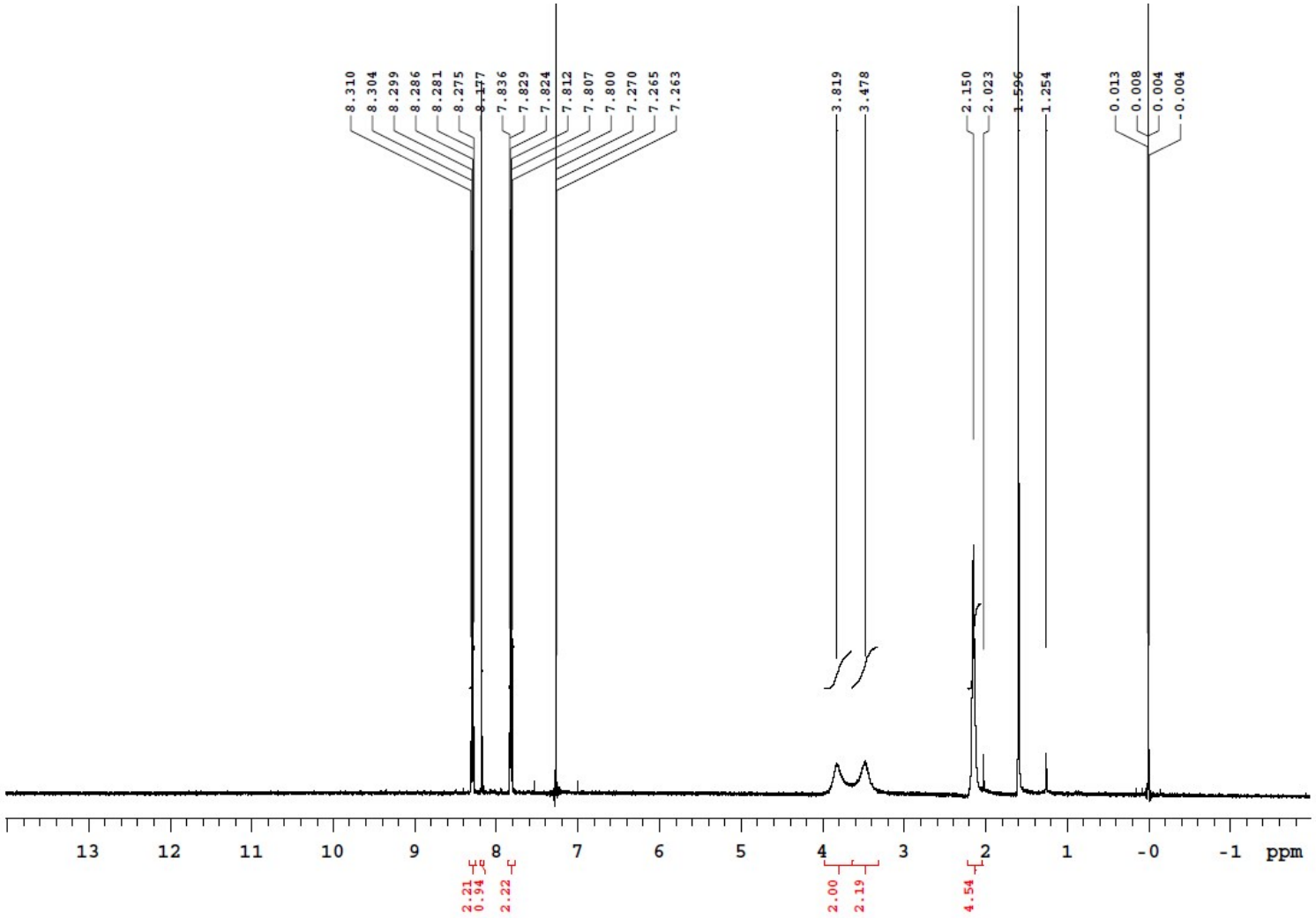

Fig. SI-17. ^{1}H NMR ($CDCl_3$, 400 MHz, 15 °C) spectrum of compound **5a.**

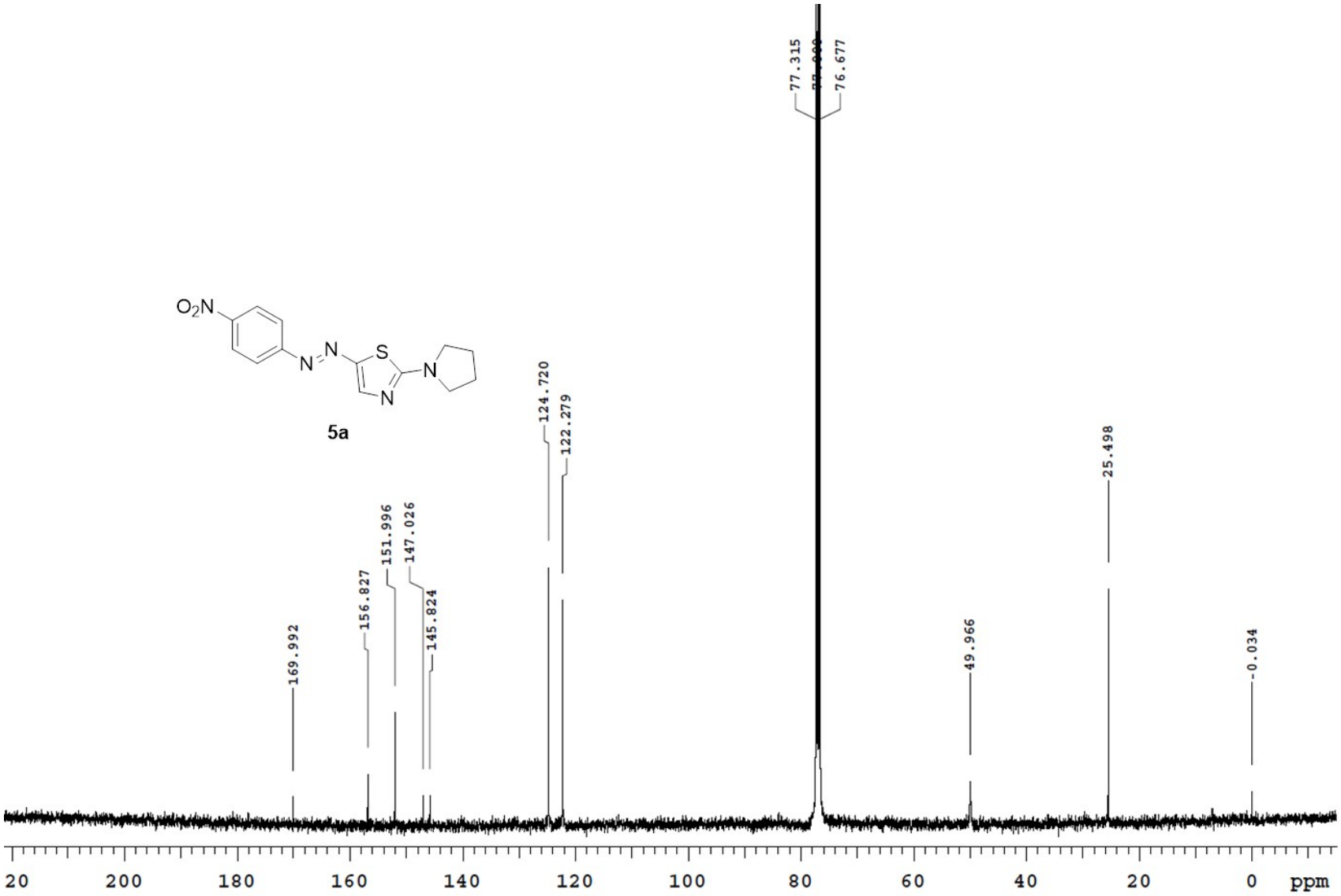

Fig. SI-18. ^{13}C NMR ($CDCl_3$, 100.56 MHz, 45 °C) spectrum of compound **5a.**

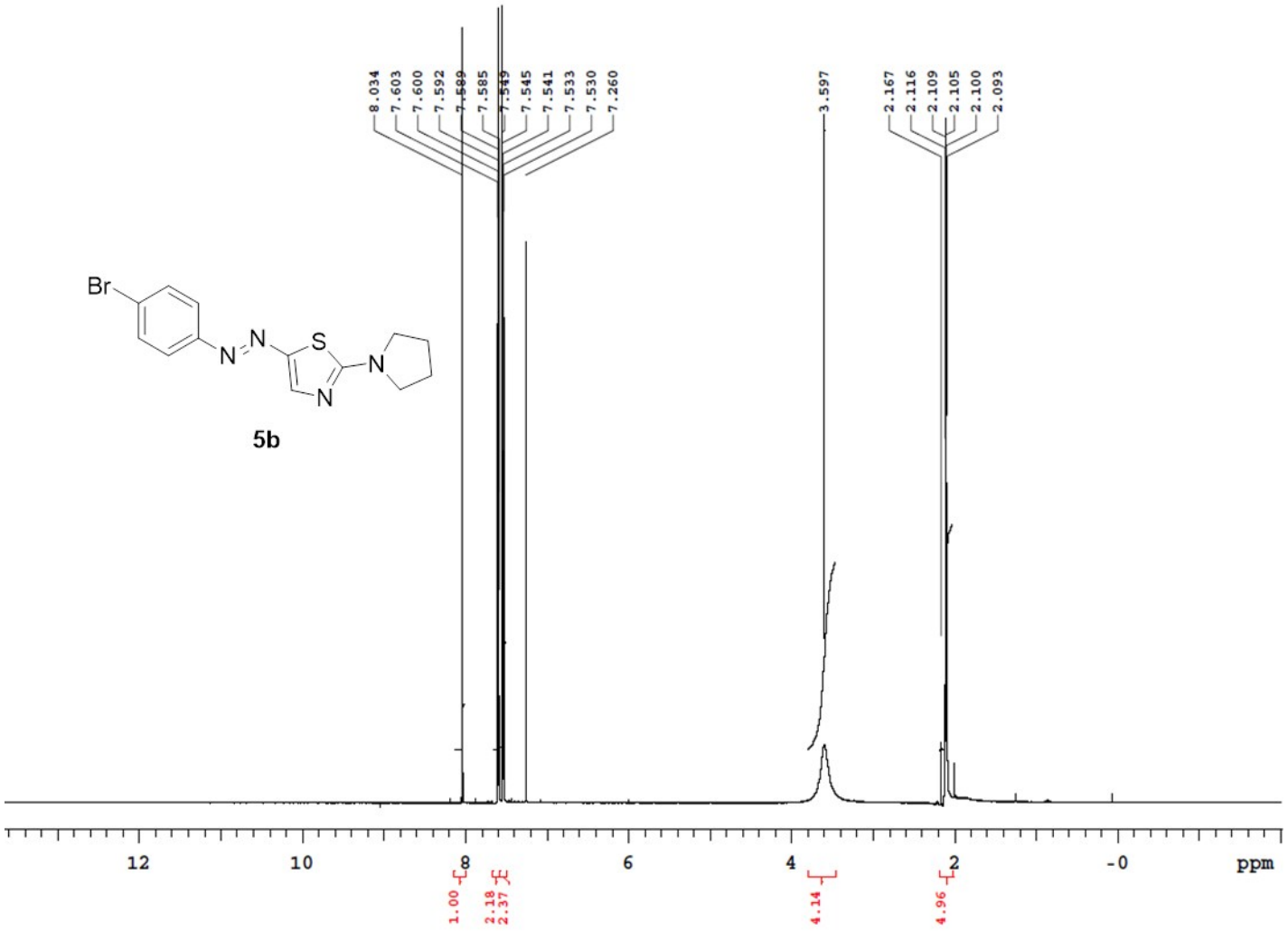

Fig. SI-19. ^{1}H NMR ($CDCl_3$, 600 MHz, 25 °C) spectrum of compound **5b.**

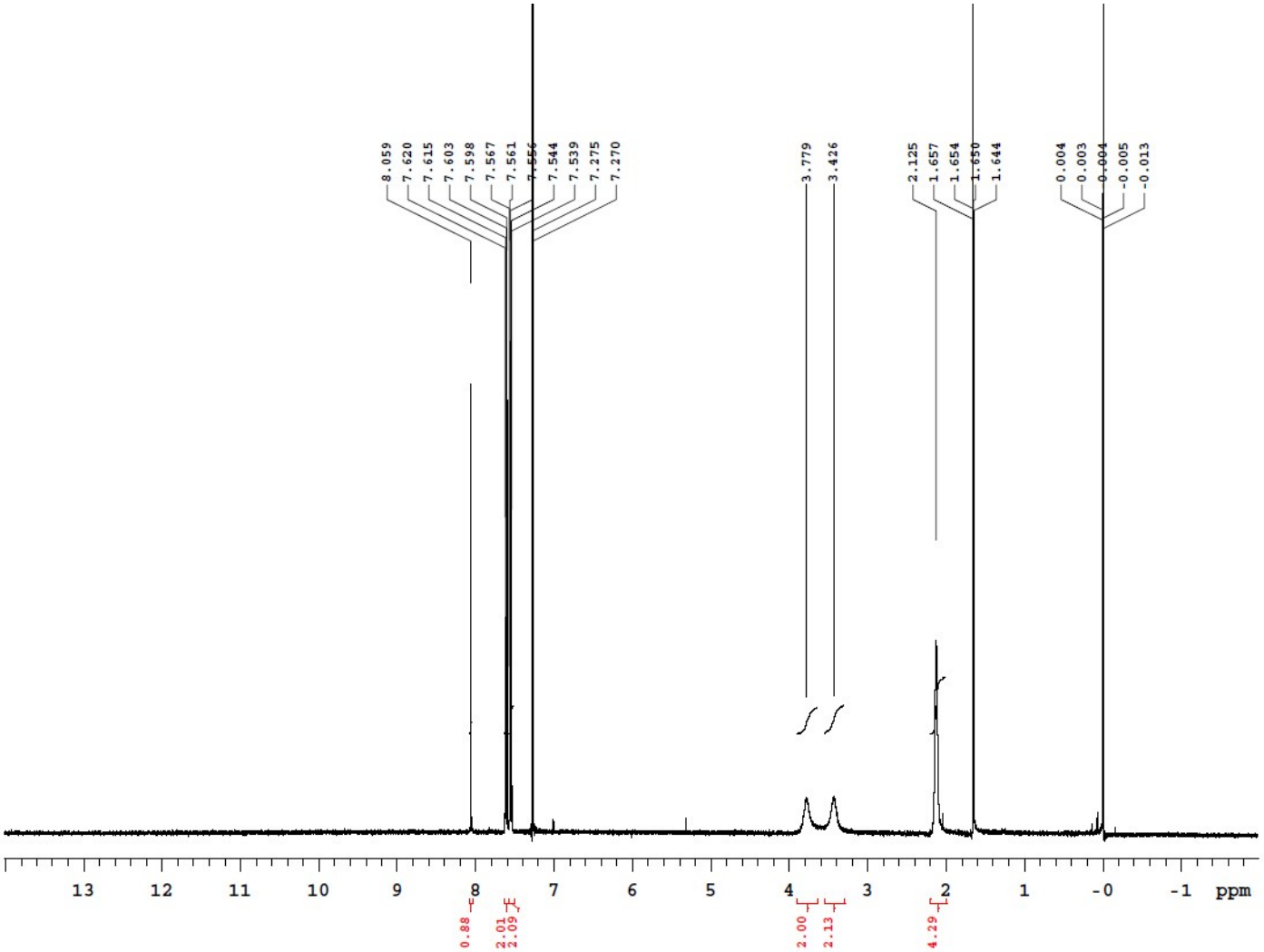

Fig. SI-20. ^{1}H NMR ($CDCl_3$, 600 MHz, -5 °C) spectrum of compound **5b.**

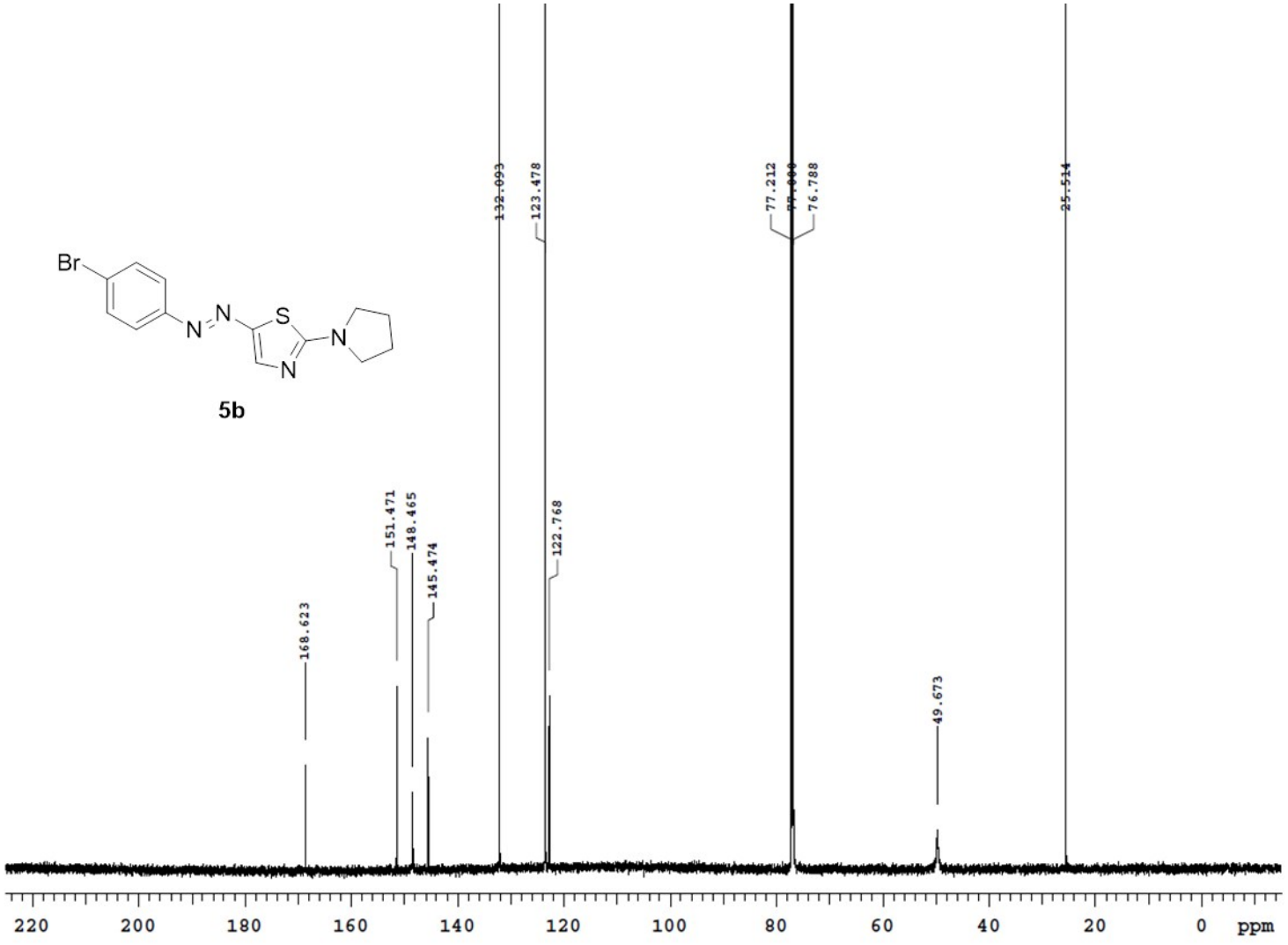

Fig. SI-21. ^{13}C NMR ($CDCl_3$, 150.8 MHz, 25 °C) spectrum of compound **5b.**

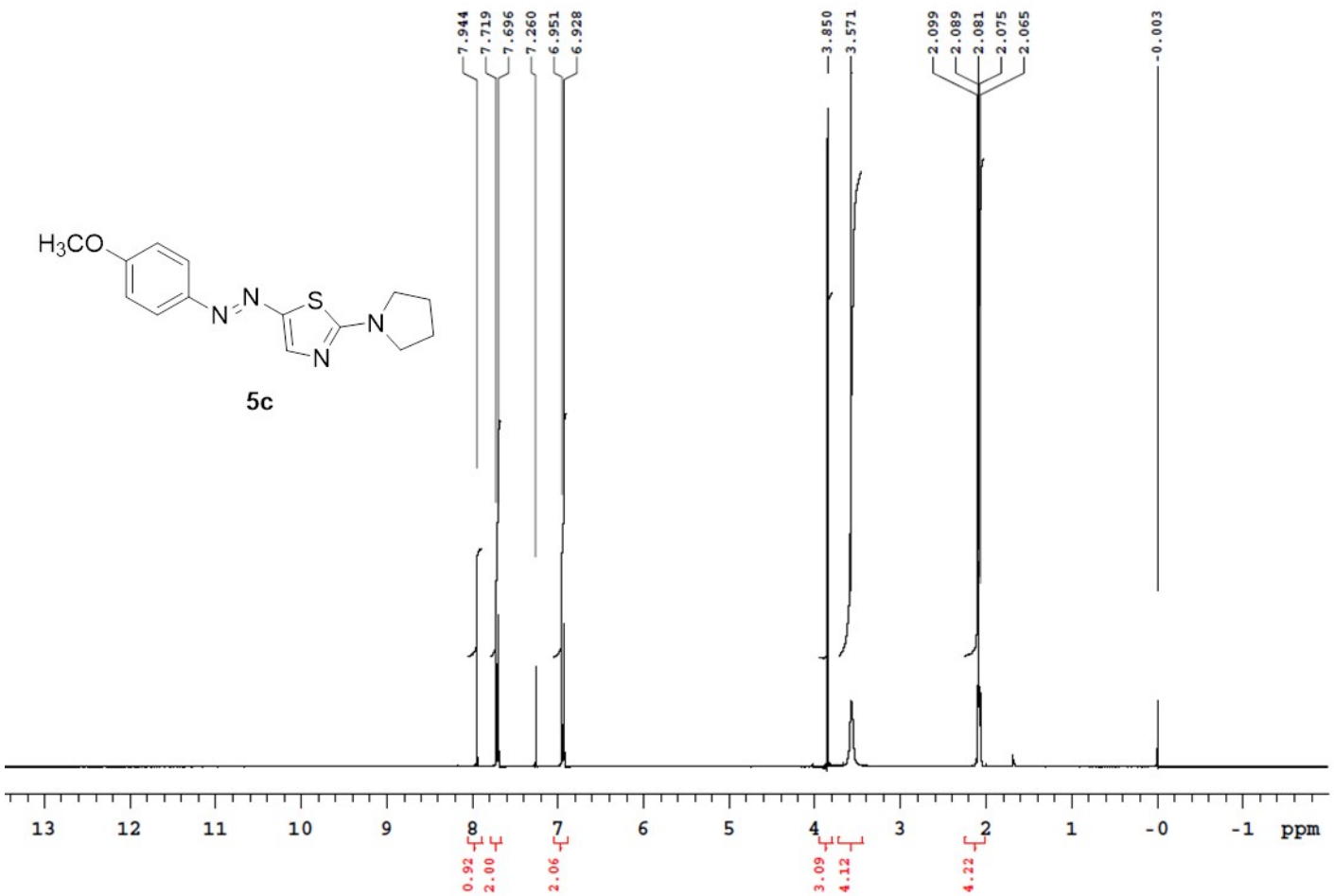

Fig. SI-22. ^{1}H NMR ($CDCl_3$, 600 MHz, 25 °C) spectrum of compound **5c**.

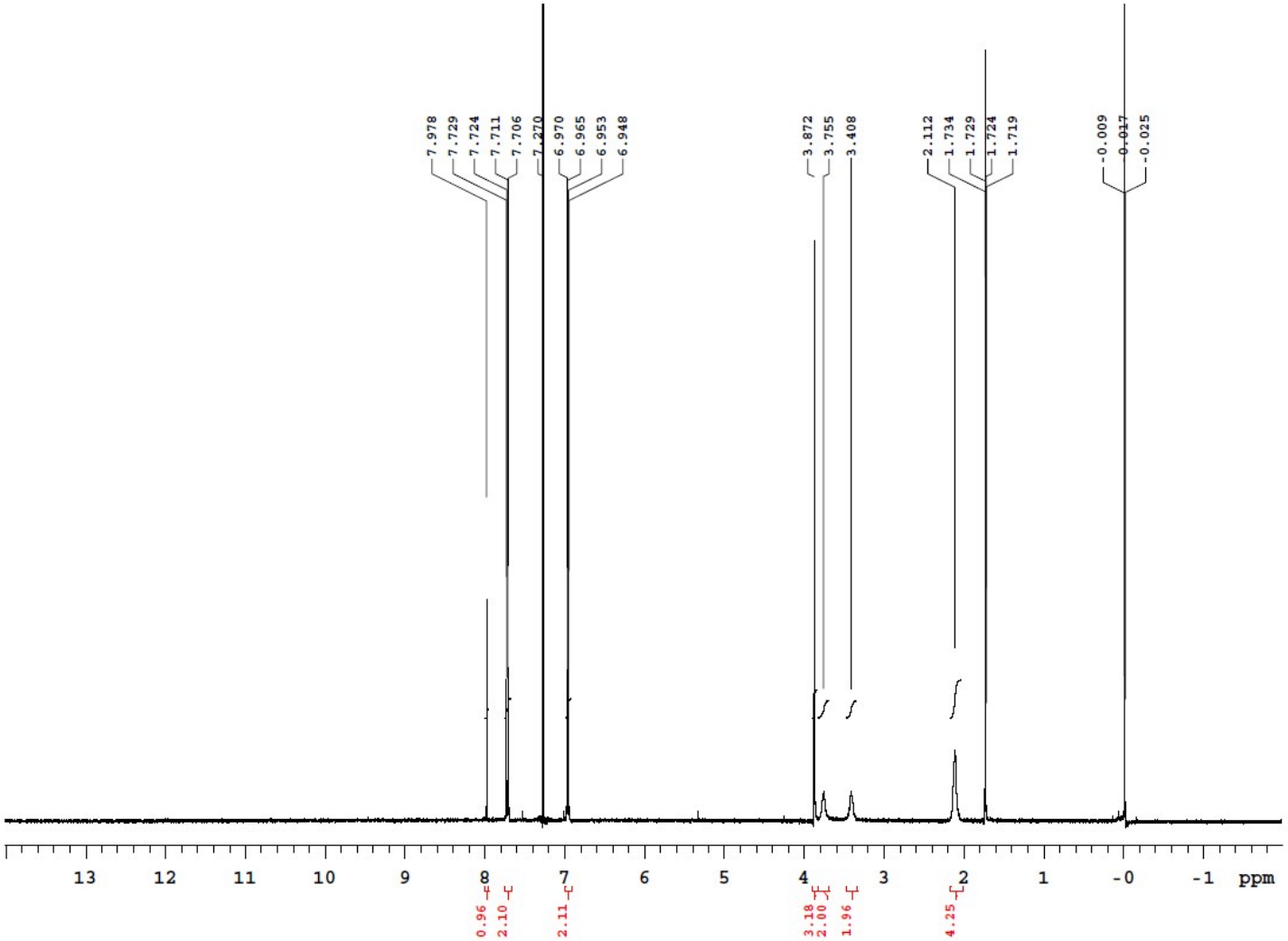

Fig. SI-23. ^{1}H NMR ($CDCl_3$, 600 MHz,-25 °C) spectrum of compound **5c**.

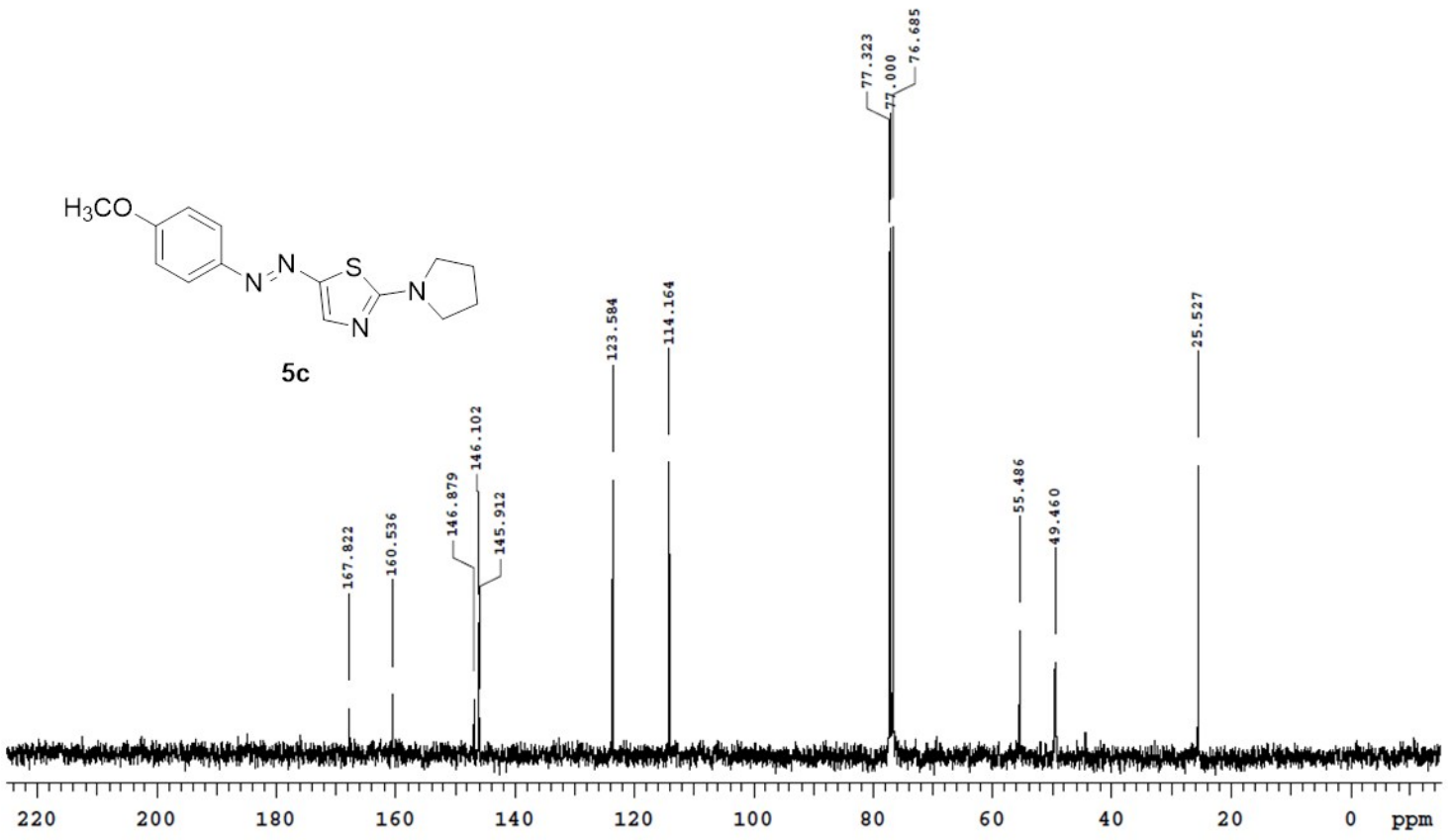

Fig. SI-24. ^{13}C NMR ($CDCl_3$, 100.56 MHz, 25 °C) spectrum of compound **5c.**

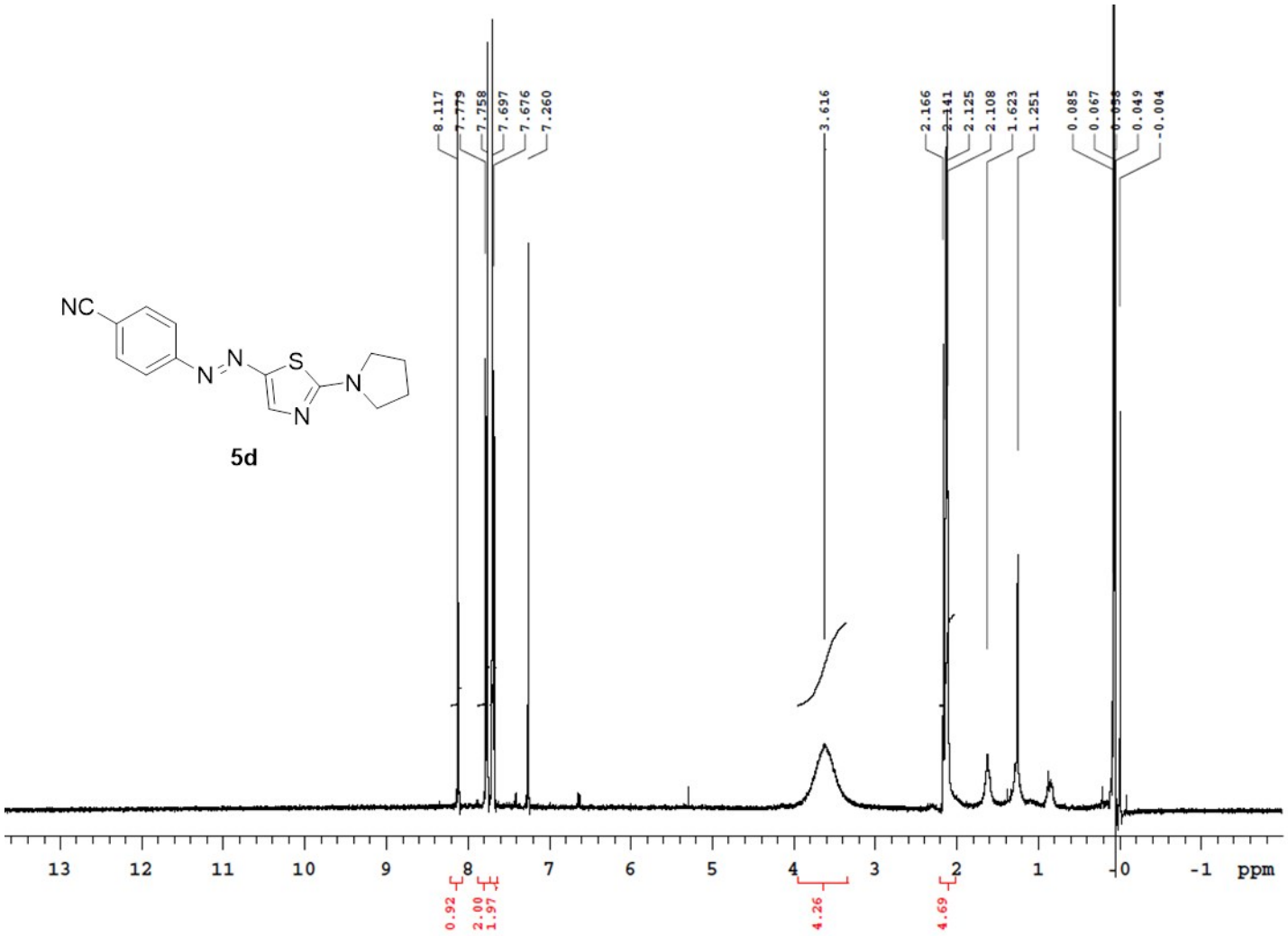

Fig. SI-25. ^{1}H NMR ($CDCl_3$, 400 MHz, 25 °C) spectrum of compound **5d.**

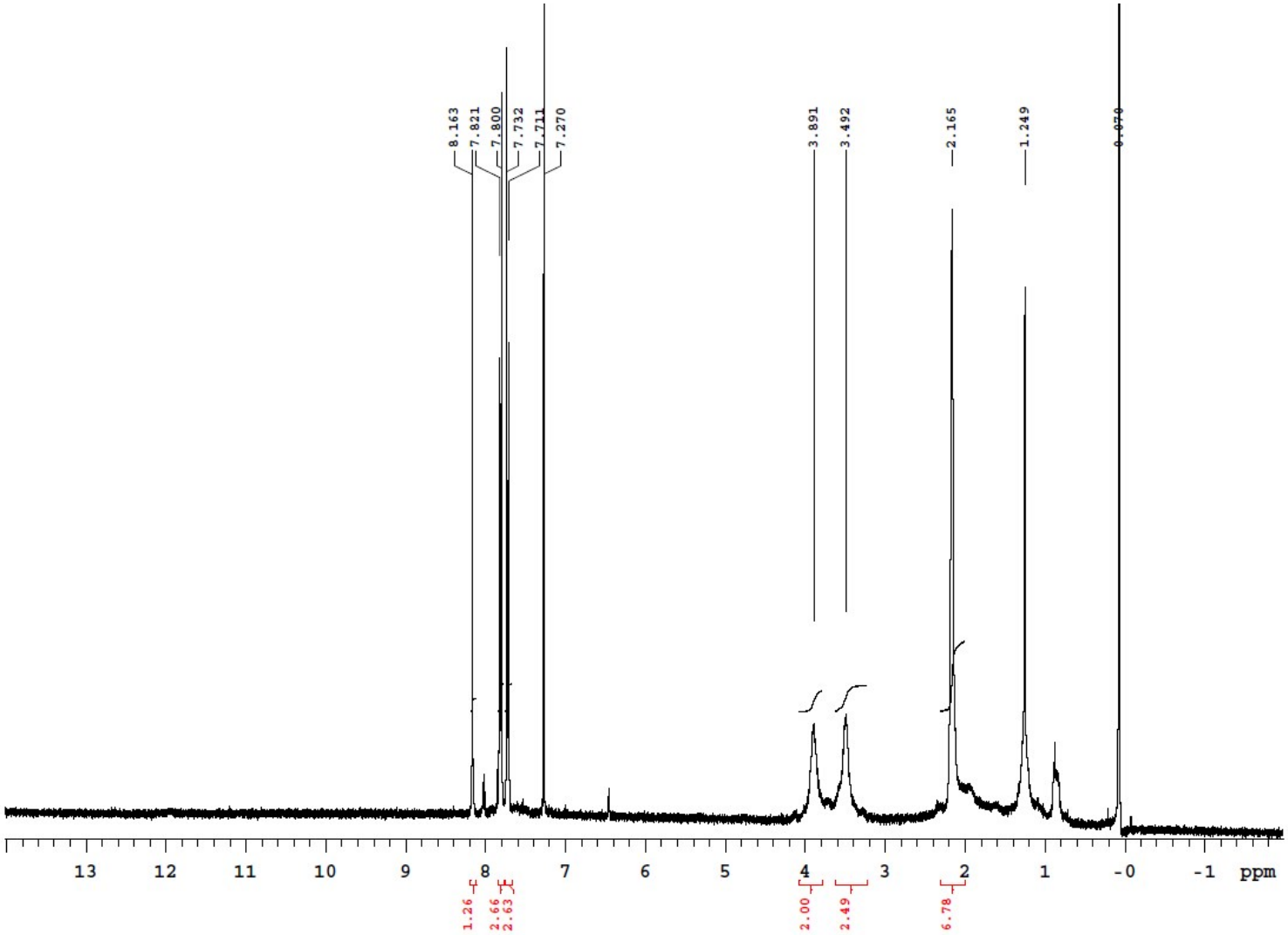

Fig. SI-26. ^{1}H NMR ($CDCl_3$, 400 MHz, 10 °C) spectrum of compound **5d.**

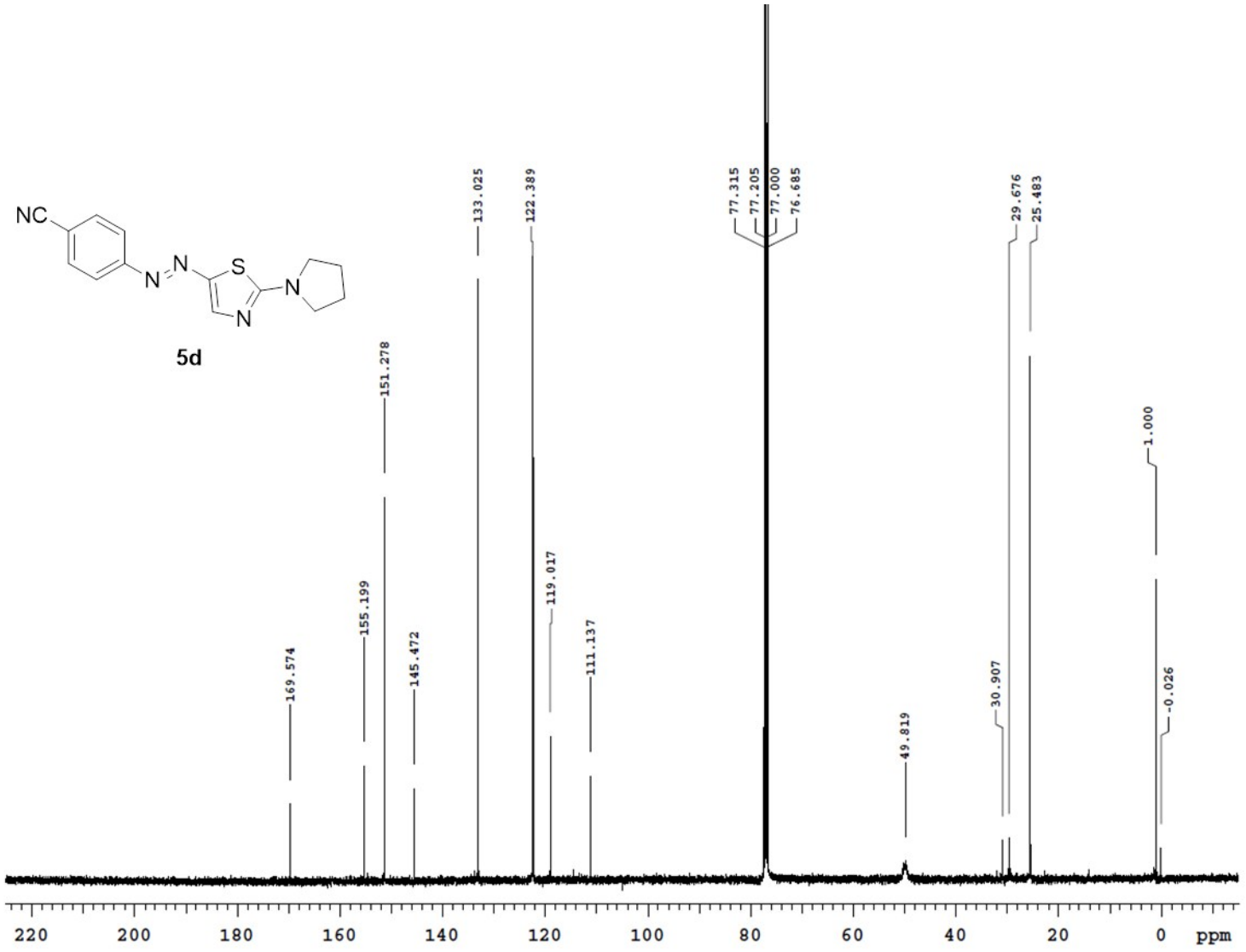

Fig. SI-27. ^{13}C NMR ($CDCl_3$, 100.56 MHz, 25 °C) spectrum of compound **5d.**

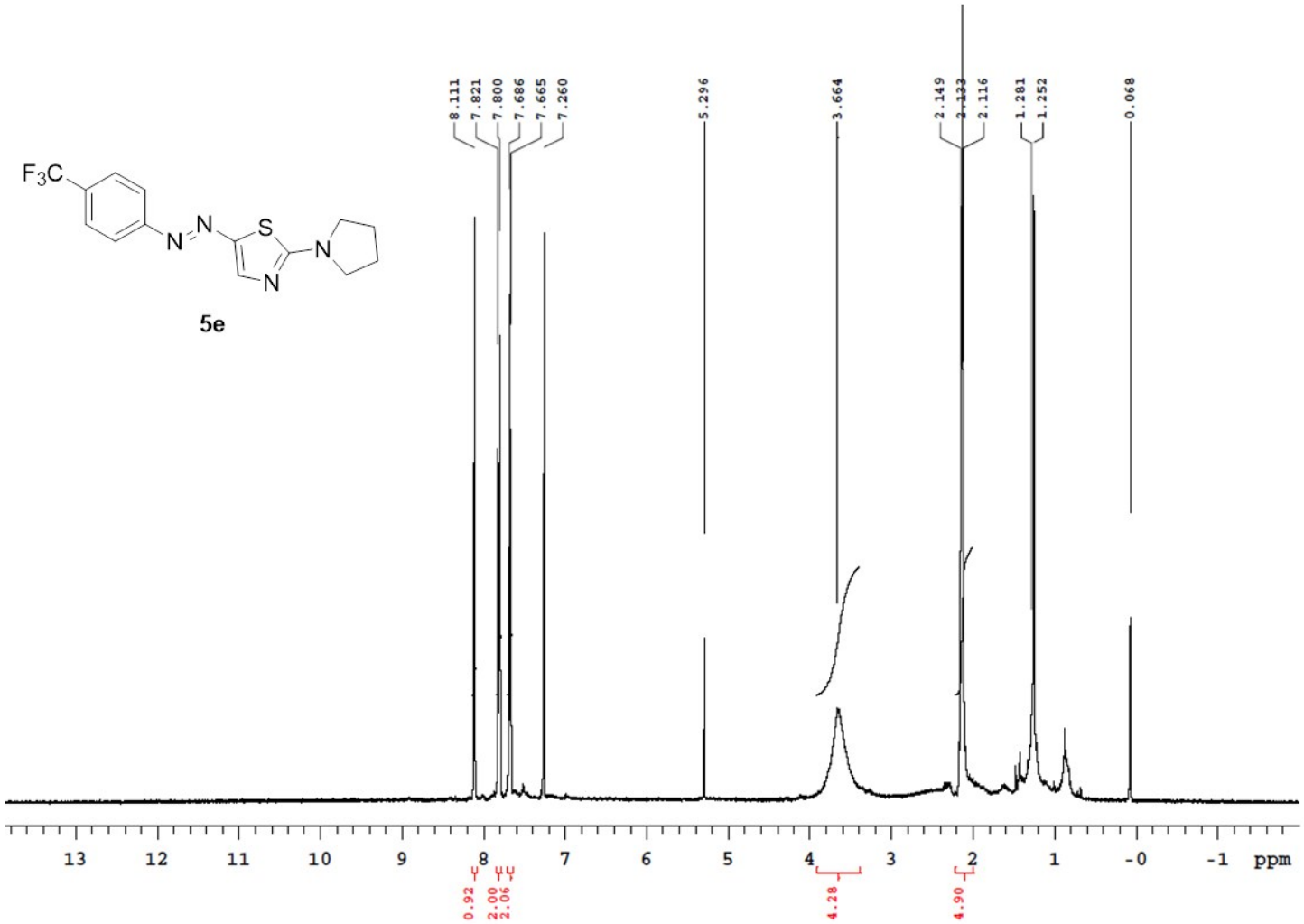

Fig. SI-28. ^{1}H NMR ($CDCl_3$, 400 MHz, 25 °C) spectrum of compound **5e.**

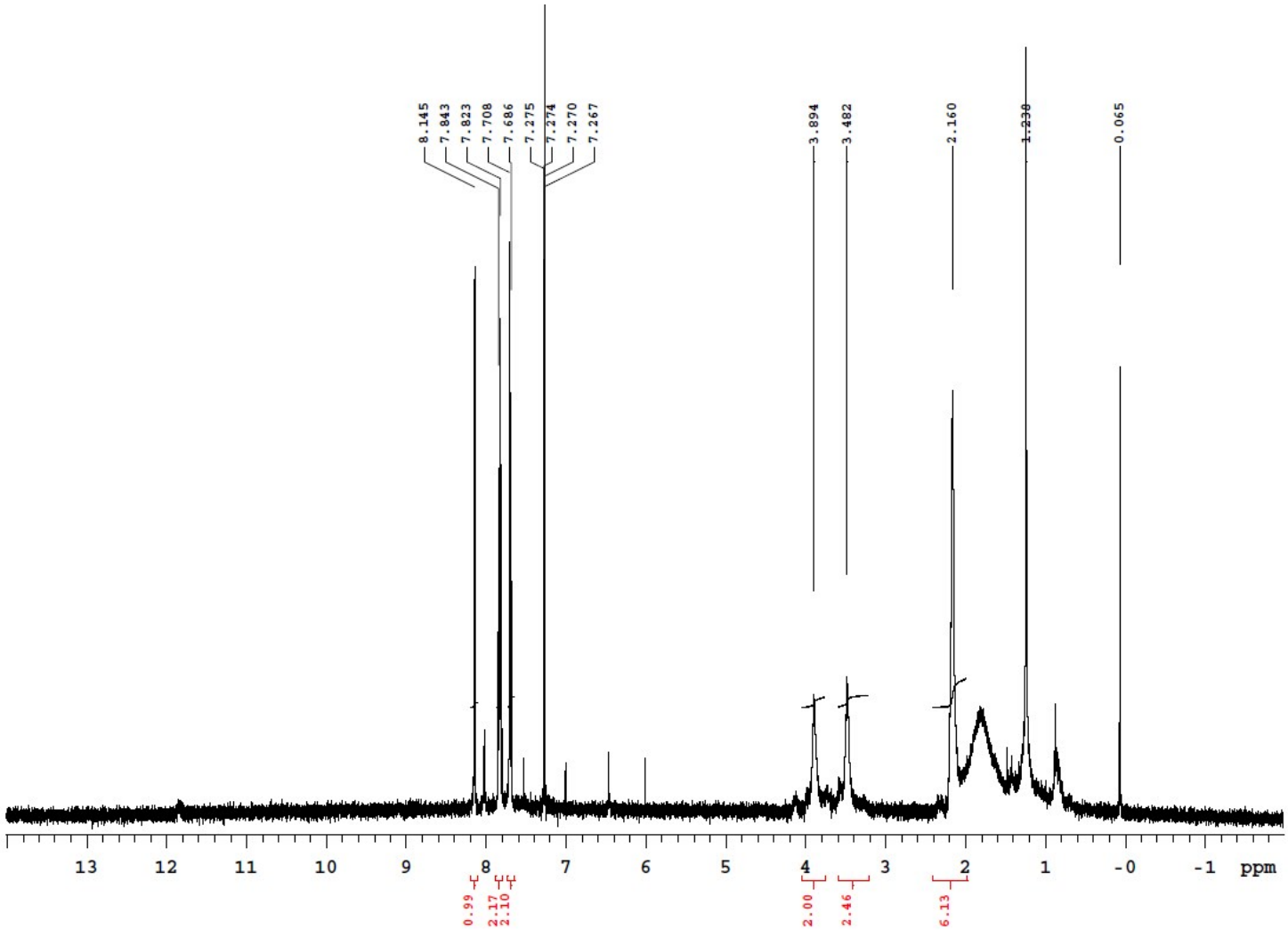

Fig. SI-29. ^{1}H NMR ($CDCl_3$, 400 MHz, -5 °C) spectrum of compound **5e.**

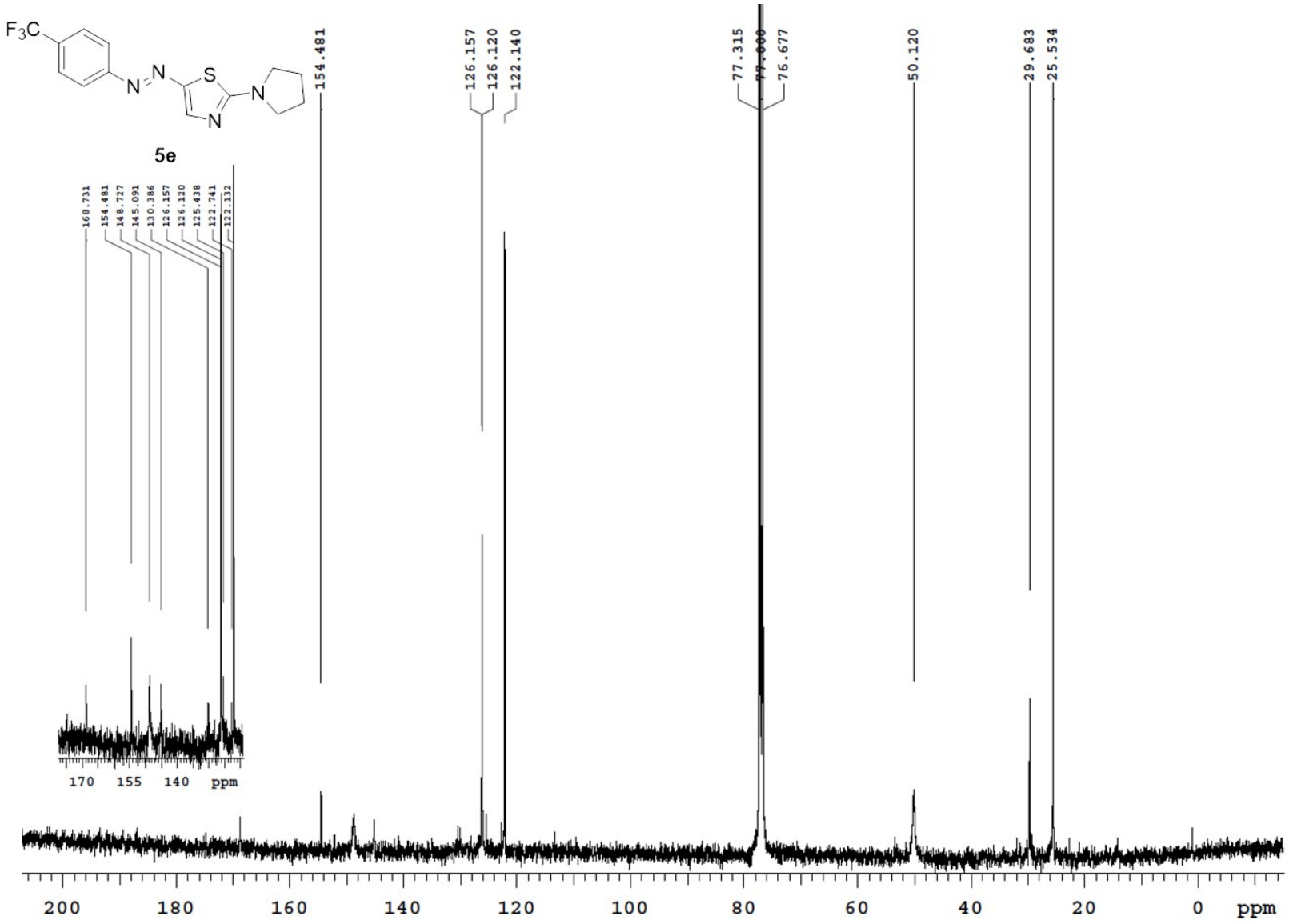

Fig. SI-30. ^{13}C NMR ($CDCl_3$, 100.56 MHz, 25 °C) spectrum, with the particular of the 170–120 ppm region, of compound **5e.**

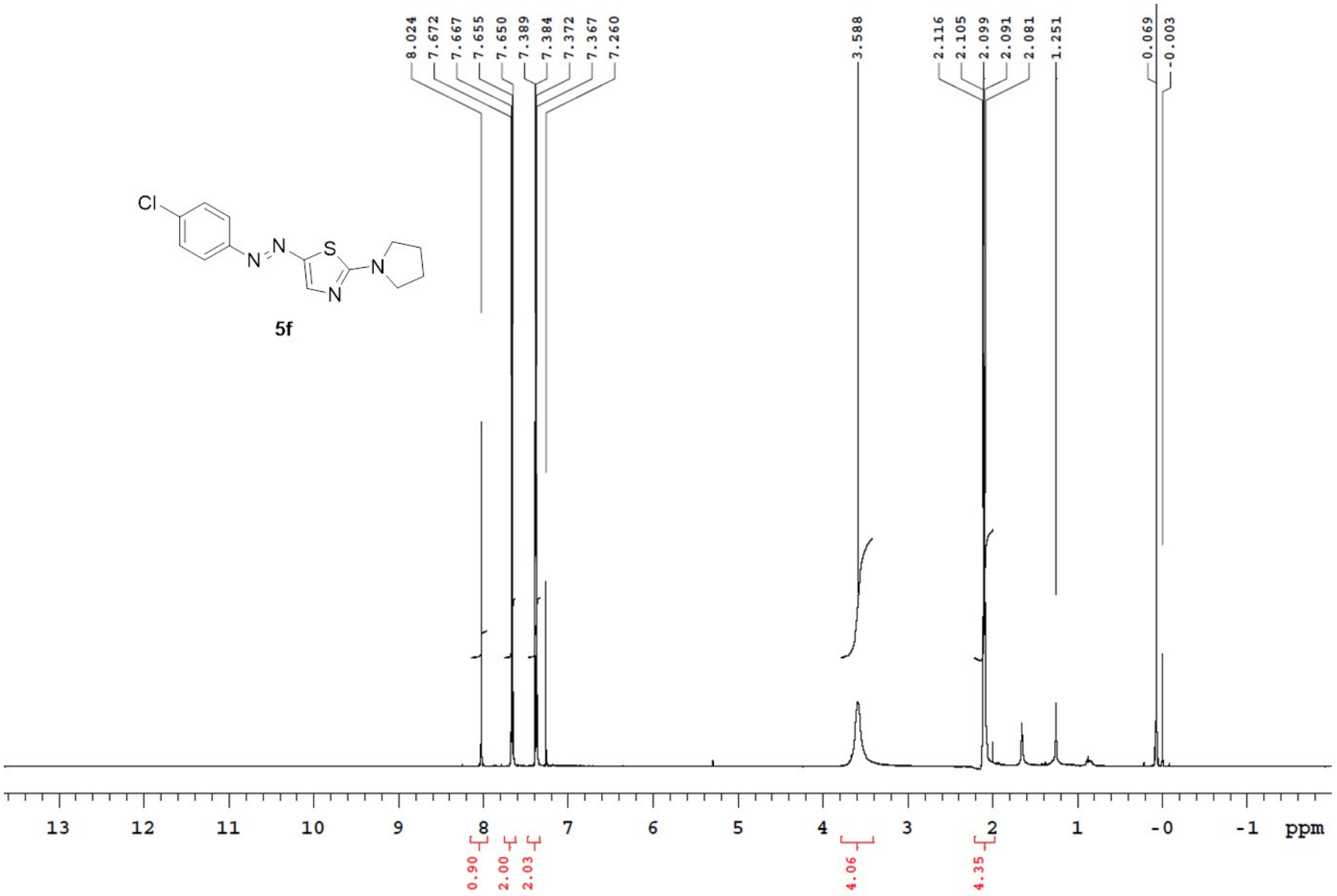

Fig. SI-31. ^{1}H NMR ($CDCl_3$, 400 MHz, 25 °C) spectrum of compound **5f.**

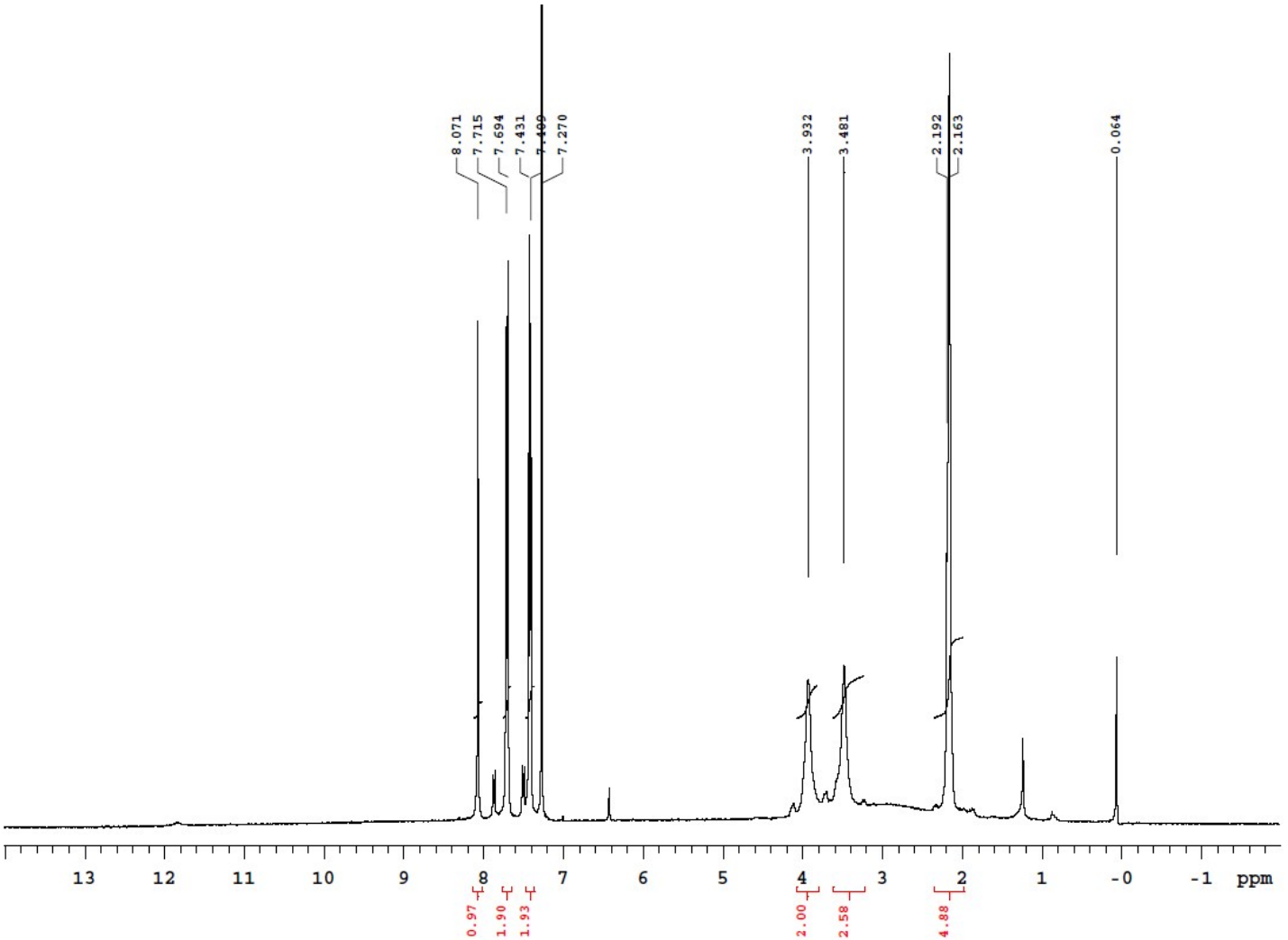

Fig. SI-32. ^{1}H NMR ($CDCl_3$, 400 MHz, -5 °C) spectrum of compound **5f.**

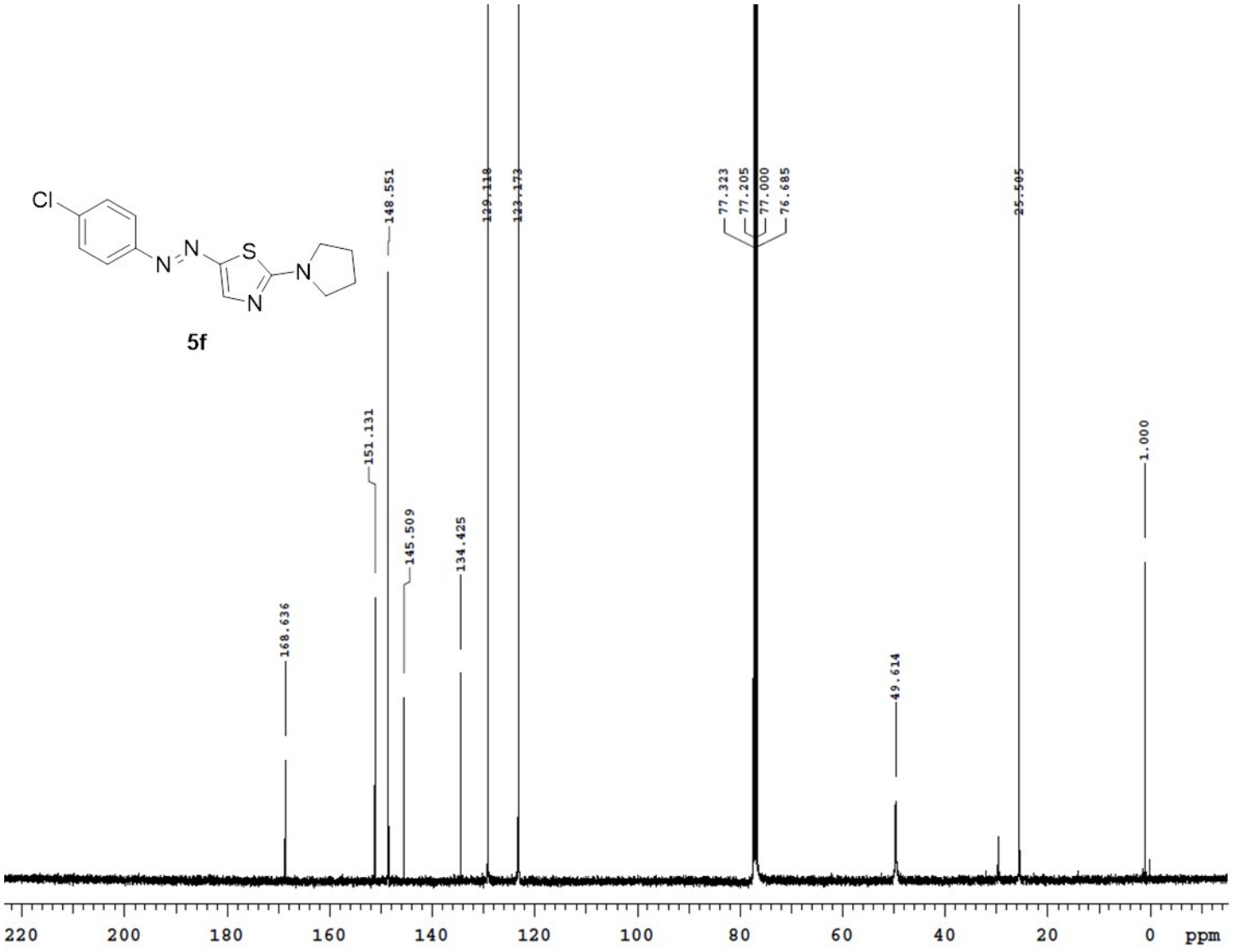

Fig. SI-33. ^{13}C NMR ($CDCl_3$, 100.56 MHz, 25 °C) spectrum with expansion of compound **5f.**

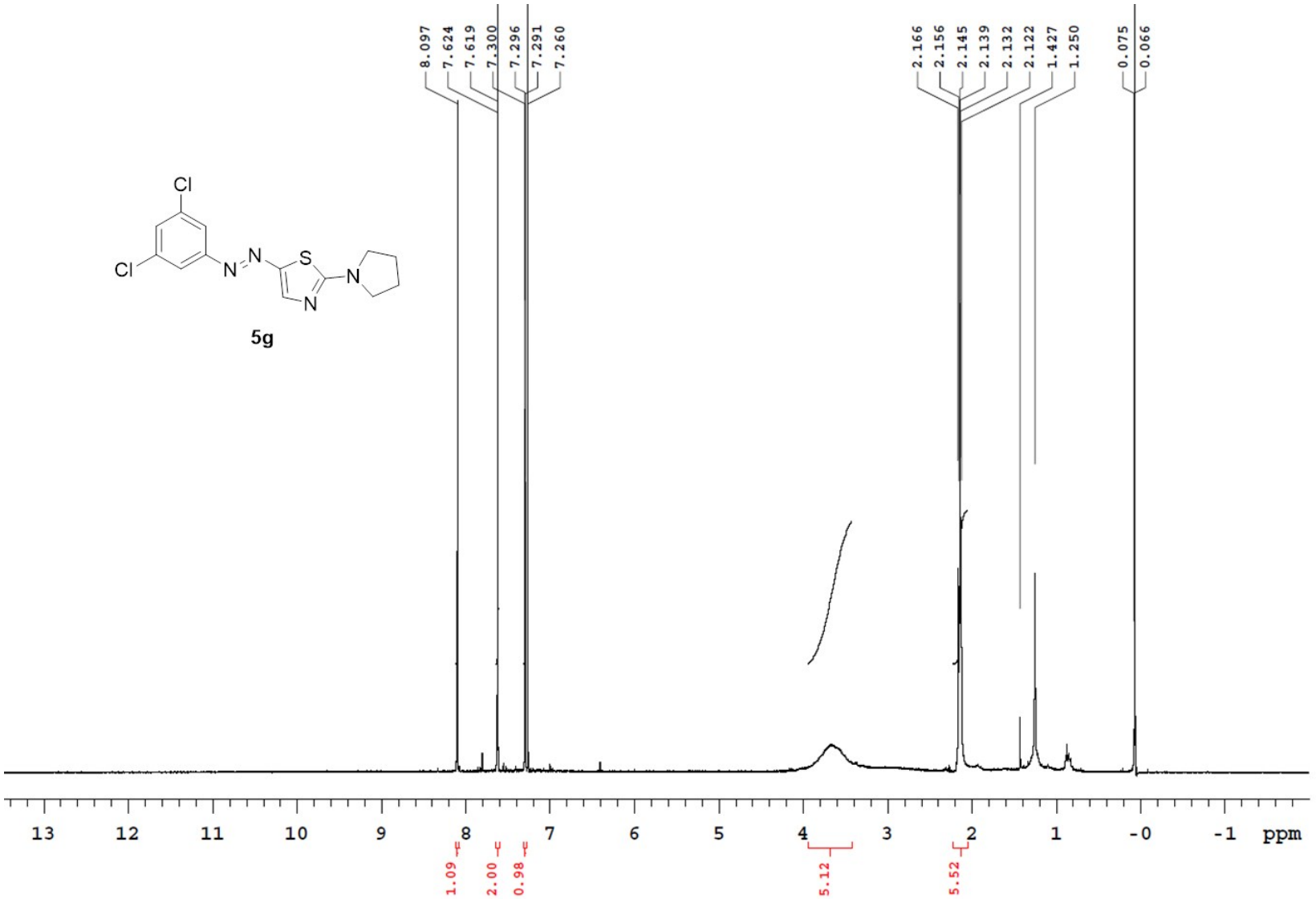

Fig. SI-34. ^{1}H NMR ($CDCl_3$, 400 MHz, 25 °C) spectrum of compound **5g.**

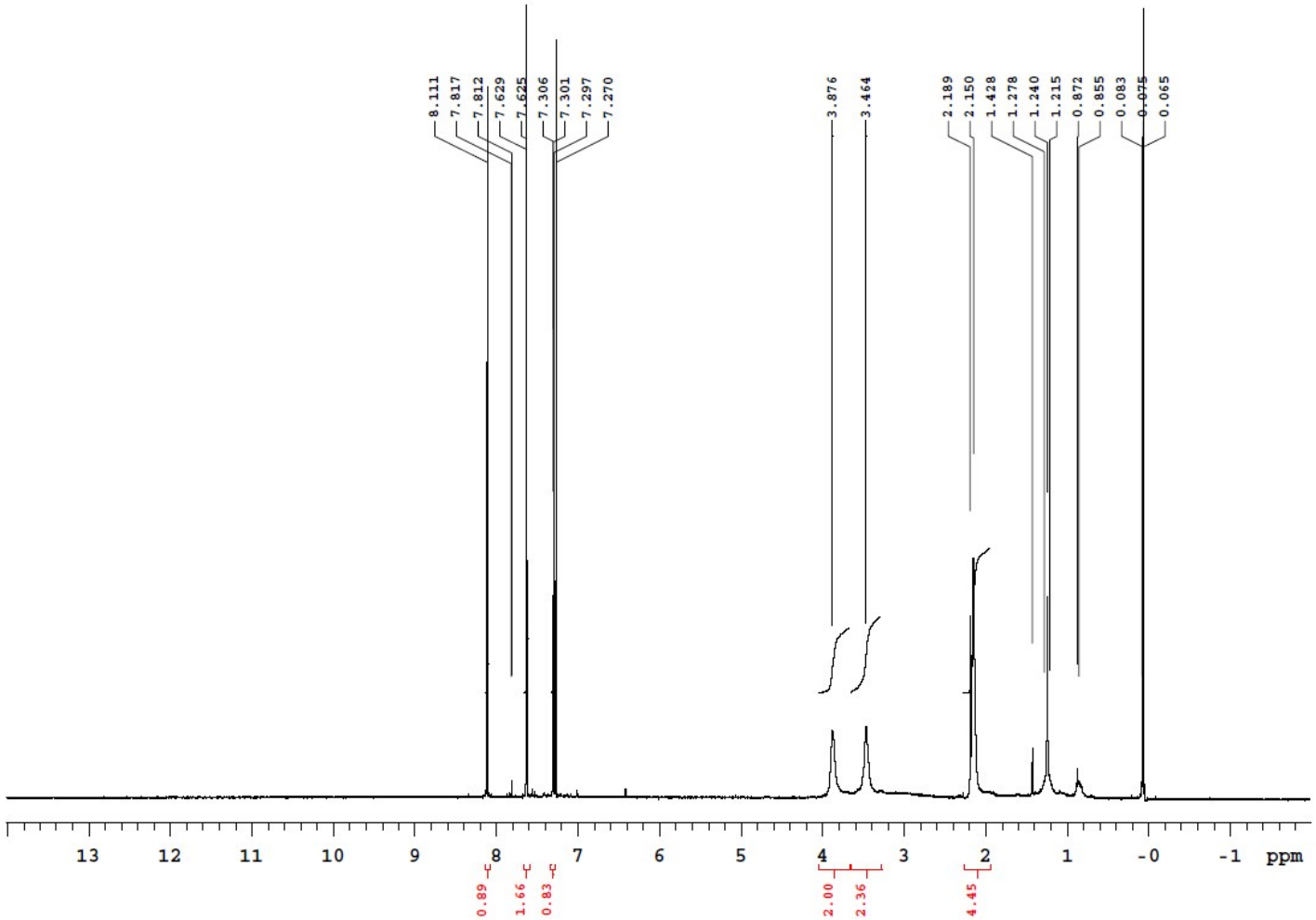

Fig. SI-35. ^{1}H NMR ($CDCl_3$, 400 MHz, 0°C) spectrum of compound **5g.**

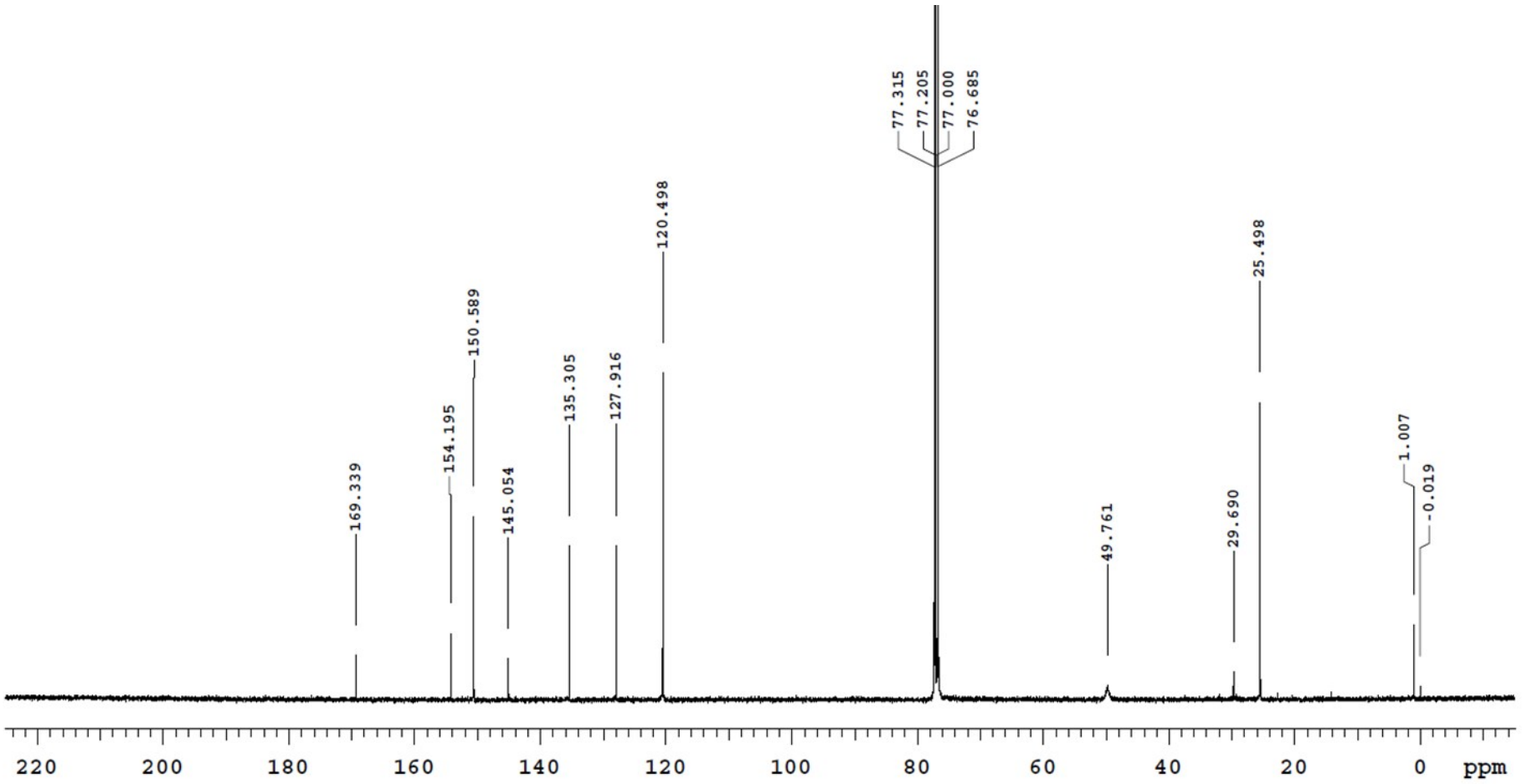

Fig. SI-36. ^{13}C NMR (100.56 MHz, $CDCl_3$, 25 °C) spectrum of compound **5g.**

Electronic-density distribution maps for 1 and 4.

In order to gain information on the reactivity of **1** and **4** towards electrophilic reagents, we carried out density functional theory (DFT) calculation. Both structures were optimized in gas phase using B3LYP[1–4] functional with 6-311+G(2d,p) basis set; the charge distribution have been calculated using the Chelp method.[5]

Figures SI-37 and SI-38 show the optimized structures mapped with Electrostatic Surface Potential (ESP) for both compound **1** and **4**. ESP is mapped on the electron-density surface where red corresponds to electron-rich and blue corresponds to electron-poor regions. It can be noted that for compound **1** the electronic density on the C-5 carbon atom is comparable to that on the nitrogen atom belonging to the thiazole ring. On the contrary, in compound **4** the electronic density on the C-5 carbon atom is considerably lower with respect to compound **1**, whereas the electronic charge is mainly localized on the endocyclic nitrogen atom, as expected because of the lack of the pyrrolidinyl group in C-4 position on going from **1** to **4**.

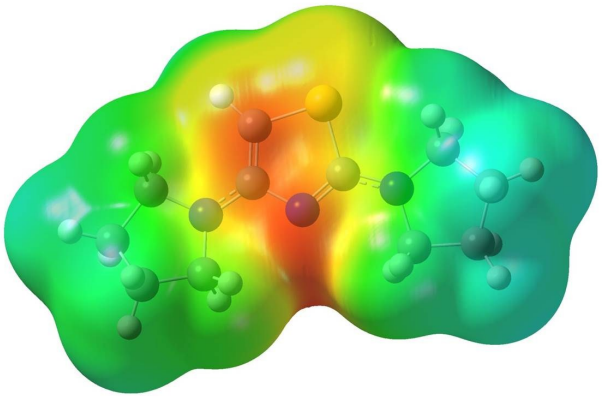

Figure SI-37. Electronic density distribution map for 2,4-*N*,*N*-dipyrrolidinylthiazole (**1**).

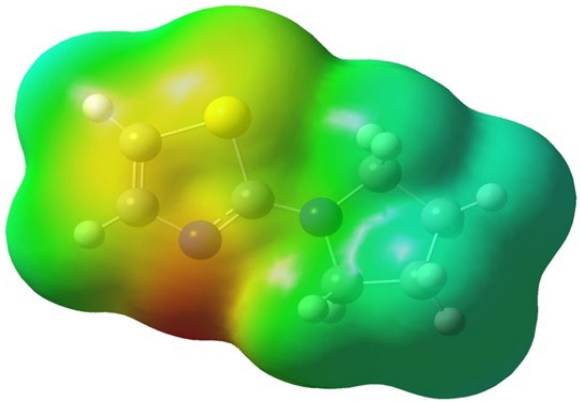

Figure SI-38. Electronic density distribution map for 2-*N*-pyrrolidinylthiazole (**4**).

In Table SI-1 are reported the values of the atomic charge on the nitrogen atom belonging to the thiazole ring (N-3) and on the C-2, C-4 and C-5 carbon atom in both compounds **1** and **4**. The presence of the pyrrolidinyl group in position 4 in compound **1** causes an increase of the negative charge on the C-5 carbon atom, much greater than the value of N-3 in both mono- and di-substituted pyrrolidinyl compounds.

Table SI-1. Charge distribution in thiazole derivatives **1** and **4**.

	N3	C2	C4	C5
2-pyrrolidinylthiazole (**4**)	-0.438	0.443	0.049	-0.113
2,4-diprrolidinylthiazole (**1**)	-0.578	0.473	0.665	-0.660

We also optimized the structure of **3a** and **3b** in gas phase using B3LYP[1–4] functional with 6-311+G(2d,p) basis set; the charge distribution have been calculated using the Chelp method.[5]

In Table SI-2 are reported the values of the atomic charge on the C-2 and C-4 carbon atom in both compounds **3a** and **3b**. The presence of the bromine / nitro substituted diazo moieties slightly decreases the charge on both C2 and C4 positions with respect to the parent compound **1** for both compounds.

Table SI-2. Charge distribution in thiazole derivatives **3a** and **3b**.

	C2	C4
3a	0.443	0.331
3b	0.450	0.227

References

1. Lee, C.; Yang, W.; Parr, R. G. *Phys. Rev. B* **1988**, *37*, 785–789.
2. Becke, A. D. *Phys. Rev. A* **1988**, *38*, 3098–3100.
3. Becke, A. D. *J. Chem. Phys.* **1993**, *98*, 5648–5652.
4. Stephens, P. J.; Devlin, F. J.; Chabalowski, C. F.; Frisch,M. J. *J. Phys. Chem.* **1994**, *98*, 11623–11627.
5. Chirlian, L. E.; Francl, M. M. *J. Comp. Chem.* **1987**, *8*, 894–905.